

FTUAM-07/10
IFT-UAM/CSIC-07-28
LPT-ORSAY-07-51

February 5, 2008

$\mu - e$ conversion in nuclei within the CMSSM seesaw: universality versus non-universality

E. Arganda^a, M. J. Herrero^a and A. M. Teixeira^b

^a*Departamento de Física Teórica C-XI and Instituto de Física Teórica C-XVI,
Universidad Autónoma de Madrid, Cantoblanco, E-28049 Madrid, Spain*

^b*Laboratoire de Physique Théorique, UMR 8627
Université de Paris-Sud XI, Bâtiment 201, F-91405 Orsay Cedex, France*

Abstract

In this paper we study $\mu - e$ conversion in nuclei within the context of the Constrained Minimal Supersymmetric Standard Model, enlarged by three right handed neutrinos and their supersymmetric partners, and where the neutrino masses are generated via a seesaw mechanism. Two different scenarios with either universal or non-universal soft supersymmetry breaking Higgs masses at the gauge coupling unification scale are considered. In the first part we present a complete one-loop computation of the conversion rate for this process that includes the photon-, Z -boson, and Higgs-boson penguins, as well as box diagrams, and compare their size in the two considered scenarios. Then, in these two scenarios we analyse the relevance of the various parameters on the conversion rates, particularly emphasising the role played by the heavy neutrino masses, $\tan\beta$, and especially θ_{13} . In the case of hierarchical heavy neutrinos, an extremely high sensitivity of the rates to θ_{13} is indeed found. The last part of this work is devoted to the study of the interesting loss of correlation between the $\mu - e$ conversion and $\mu \rightarrow e\gamma$ rates that occurs in the non-universal scenario. In the case of large $\tan\beta$ and light H^0 Higgs boson, an enhanced ratio of the $\mu - e$ to $\mu \rightarrow e\gamma$ rates, with respect to the universal case is found, and this could be tested with the future experimental sensitivities.

1 Introduction

Neutrino physics, in particular neutrino oscillations and the measured neutrino mass differences, strongly manifest that Nature does not conserve the lepton flavour quantum number in the neutrino sector [1, 2]. However, it is not known yet if lepton flavour violation (LFV) also occurs in the charged lepton sector. If such is the case, one still has to address if LFV in the neutral and charged lepton sectors arises from a common or different origin. It is well known that if the Standard Model of Particle Physics (SM) is minimally extended in order to accommodate the present data on neutrino masses and mixings, the corresponding loop induced LFV in the charged lepton sector (exclusively induced from neutrino oscillations) is extremely tiny and hopeless to be experimentally observed. Therefore, a potential future measurement of LFV in the charged lepton sector will provide a unique insight into the nature of new physics beyond the SM (for a review, see [3]).

Among the various candidates for physics beyond the SM that produce potentially observable effects in LFV processes, one of the most appealing are Supersymmetric (SUSY) extensions of the SM, where a seesaw mechanism [4, 5] is implemented to generate neutrino masses. In these SUSY-seesaw models a new source of LFV appears in the off-diagonal elements of the slepton mass matrices, which can be radiatively generated. The size of these elements is governed by the strength of the neutrino Yukawa couplings and, in the case of Majorana neutrinos, the latter can be large, of the order of one. The LFV effects in the charged lepton processes are then induced by flavour violating slepton-lepton interactions, appearing in SUSY-loop diagrams mediated by sleptons [6].

Concerning the LFV processes, in our work we will focus on those which involve flavour transitions between the first and second generation of charged leptons. At present, the most relevant $\mu - e$ flavour violating processes are $\mu \rightarrow e\gamma$, $\mu \rightarrow 3e$ and $\mu - e$ conversion in nuclei. The current experimental bounds on the muon decays are $\text{BR}(\mu \rightarrow e\gamma) < 1.2 \times 10^{-11}$ [7] and $\text{BR}(\mu \rightarrow 3e) < 1.0 \times 10^{-12}$ [8]. Regarding $\mu - e$ conversion in heavy nuclei, the most stringent constraints arise for Titanium and Gold, respectively with $\text{CR}(\mu - e, \text{Ti}) < 4.3 \times 10^{-12}$ [9] and $\text{CR}(\mu - e, \text{Au}) < 7 \times 10^{-13}$ [10]. In the future, one expects significant improvements in the sensitivities to these LFV rates. For instance, MEG aims at reaching a sensitivity for $\mu \rightarrow e\gamma$ of 10^{-13} [11] in the very near future, which could further be improved to 10^{-14} in the next 4-5 years [12]. Although the situation for $\text{BR}(\mu \rightarrow 3e)$ is less certain, one does not expect the sensitivities to better $10^{-13} - 10^{-14}$ [12]. Undoubtedly, the most challenging prospects concern the experimental sensitivities to $\mu - e$ conversion in Titanium nuclei. The dedicated J-PARC experiment PRISM/PRIME has announced a remarkable improvement, albeit in a

farer future, of 10^{-18} [13].

In this paper we will focus on $\mu - e$ conversion in nuclei, working in the context of the Minimal Supersymmetric Standard Model (MSSM) enlarged by three right handed neutrinos and their corresponding SUSY partners, where a type-I seesaw mechanism [4] is implemented. To reduce the number of unknown parameters in the SUSY sector, we choose to work in the so-called constrained MSSM (CMSSM)(for a review see for instance [14]), assuming universality of the soft-SUSY breaking parameters at the scale of gauge coupling unification, $M_X \sim 2 \times 10^{16}$ GeV. An interesting departure from the CMSSM-seesaw can be obtained by relaxing the universality hypothesis for the soft SUSY breaking masses of the Higgs sector. This partially constrained MSSM is commonly referred to as the Non Universal Higgs Mass (NUHM) scenario [15], and its enlarged version (including right handed neutrinos and sneutrinos) will be here designated NUHM-seesaw.

Within the context of the CMSSM- and NUHM-seesaw, we conduct here a thorough analysis of the predictions for the $\mu - e$ conversion rates in nuclei. The present computation is the first to include the *full* set of SUSY one-loop diagrams (photon, Z - and Higgs-boson mediated, as well as box diagrams), and to be strictly done in terms of physical eigenstates for the exchanged SUSY particles. For all scenarios here addressed, we obtain the low-energy parameters by numerically solving the full renormalisation group equations (RGEs), including the neutrino and sneutrino sectors. The photon and Z -boson mediated penguins, as well as the vector contributions from box diagrams were first computed in the CMSSM-seesaw in [16]. Here we have confirmed their analytical results for the photon-mediated and box contributions, correcting the analytical expressions for the Z -boson mediated processes. We further added the scalar contributions from box diagrams and the Higgs-mediated contributions, and improved the computation, by considering in the numerical analysis the possibility of either degenerate or hierarchical heavy neutrino spectrum, and by fitting the light neutrino parameters to the present data.

The effects of the Higgs-mediated contribution on $\mu - e$ conversion rates were firstly investigated in [17], in the context of a SUSY-seesaw with degenerate heavy neutrinos, working in the effective Lagrangian approximation and in the $SU(2)_L \times U(1)_Y$ limit. It was observed that the Higgs-mediated LFV diagrams could provide the dominant contribution for the large $\tan\beta$ regime and for small masses of the heavy Higgs scalar, owing to a $\tan^6\beta$ enhancement and $(m_{H^0})^{-4}$ dependence of the conversion rates. By comparing the latter with the corresponding $\mu \rightarrow e\gamma$ rates for large universal SUSY-breaking mass values, $M_0, M_{1/2} \sim \mathcal{O}(1 \text{ TeV})$, they further showed that the ratio of observables $\text{CR}(\mu - e, \text{Al})/\text{BR}(\mu \rightarrow e\gamma)$ could be enhanced from a value of $\mathcal{O}(\alpha)$ (within the usual dominant photon-mediated case)

to $\mathcal{O}(10^{-1})$ for extreme values of $\tan\beta = 60$, $M_R = 10^{14}$ GeV and $m_{H^0} \sim 100$ GeV.

In the present work we will explore in full detail the various contributions to the $\mu - e$ conversion rates and study the dependence on all parameters entering in the considered MSSM-seesaw framework. In addition to the relevant role played by the mass of the right handed neutrinos, m_{N_i} , the soft masses M_0 , $M_{1/2}$ (and $M_{H_{1,2}}$ for the NUHM-seesaw), and $\tan\beta$, we will show that the light neutrino mixing angle θ_{13} has an important impact on $\text{CR}(\mu - e, \text{Nucleus})$. The conversion rates turn out to be very sensitive to this angle, varying in many orders of magnitude (up to five in the case of hierarchical heavy neutrinos) for θ_{13} values within the present experimentally allowed region $0^\circ \leq \theta_{13} \leq 10^\circ$ [18]. We will further verify that with the future sensitivity of JPARC ($\mathcal{O}(10^{-18})$) [13] most of the parameter space could be covered.

On the other hand, the comparison between the predictions obtained for the CMSSM-seesaw and the NUHM-seesaw cases will allow us to draw interesting conclusions about the departure from the strongly correlated behaviour of $\text{CR}(\mu - e, \text{Nucleus})$ and $\text{BR}(\mu \rightarrow e\gamma)$, as predicted in photon-dominated scenarios (as is the case of the CMSSM-seesaw). In the latter scenario, the ratio of the two rates was found to be at most $1/160$ for $\tan\beta = 50$ [19]. In contrast, we will discuss here particular scenarios in the NUHM-seesaw, where the ratio $\text{CR}(\mu - e, \text{Ti})/\text{BR}(\mu \rightarrow e\gamma)$ is indeed enhanced with respect to the universal case, by as much as one order of magnitude, in agreement with the approximate results of [17].

One of the most challenging tasks in this $\mu - e$ conversion process will be to disentangle between the different scenarios for new physics if a measurement is finally obtained. Indeed, it has been already noticed in early works [20] that $\mu - e$ conversion could constrain new physics more stringently than $\mu \rightarrow e\gamma$. We will see here that this is the case in the NUHM scenario. Furthermore, we will also show that, with the expected sensitivities for Titanium of $\mathcal{O}(10^{-18})$, one could distinguish CMSSM- from NUHM- seesaw scenarios by extracting the scalar contribution to the $\text{CR}(\mu - e, \text{Ti})$ rates.

The paper is organised as follows. In Section 2 we review the most relevant features of the SUSY-seesaw scenario. The analytical results of the $\mu - e$ conversion rates are presented in Section 3. Section 4 is devoted to the numerical results for both CMSSM-seesaw and NUHM-seesaw scenarios. An extensive discussion about the sensitivities to the various parameters in these two scenarios is also included. Finally, the conclusions are summarised in Section 5.

2 The SUSY-seesaw scenario

The leptonic superpotential containing the relevant terms to describe a type-I SUSY seesaw is given by

$$W = \hat{N}^c Y_\nu \hat{L} \hat{H}_2 + \hat{E}^c Y_l \hat{L} \hat{H}_1 + \frac{1}{2} \hat{N}^c m_M \hat{N}^c, \quad (1)$$

where \hat{N}^c are the additional superfields that contain the three right-handed neutrinos ν_{R_i} and their scalar partners $\tilde{\nu}_{R_i}$. The lepton Yukawa couplings $Y_{l,\nu}$ and the Majorana mass m_M are 3×3 matrices in lepton flavour space. From now on, we will assume that we are in a basis where Y_l and m_M are diagonal.

After electroweak (EW) symmetry breaking, the charged lepton and Dirac neutrino mass matrices can be written as

$$m_l = Y_l v_1, \quad m_D = Y_\nu v_2, \quad (2)$$

where v_i are the vacuum expectation values (VEVs) of the neutral Higgs scalars, with $v_{1(2)} = v \cos(\sin)\beta$ and $v = 174$ GeV.

The 6×6 neutrino mass matrix is given by

$$M^\nu = \begin{pmatrix} 0 & m_D^T \\ m_D & m_M \end{pmatrix}. \quad (3)$$

The eigenvalues of M^ν are the masses of the six physical Majorana neutrinos. In the seesaw limit, the three right-handed masses are much heavier than the EW scale, $m_{M_i} \gg v$, and one obtains three light and three heavy states, ν_i and N_i , respectively.

Block-diagonalisation of the neutrino mass matrix of Eq. (3), leads (at lowest order in the $(m_D/m_M)^n$ expansion) to the standard seesaw equation for the light neutrino mass matrix,

$$m_\nu = -m_D^T m_M^{-1} m_D. \quad (4)$$

Since we are working in a basis where m_M is diagonal, the heavy eigenstates are then given by

$$m_N^{\text{diag}} = m_M = \text{diag}(m_{N_1}, m_{N_2}, m_{N_3}). \quad (5)$$

The matrix m_ν can be diagonalised by the Maki-Nakagawa-Sakata unitary matrix U_{MNS} [21, 22], leading to the following masses for the light physical states

$$m_\nu^{\text{diag}} = U_{\text{MNS}}^T m_\nu U_{\text{MNS}} = \text{diag}(m_{\nu_1}, m_{\nu_2}, m_{\nu_3}). \quad (6)$$

Here we use the standard parameterisation for U_{MNS} given by

$$U_{\text{MNS}} = \begin{pmatrix} c_{12} c_{13} & s_{12} c_{13} & s_{13} e^{-i\delta} \\ -s_{12} c_{23} - c_{12} s_{23} s_{13} e^{i\delta} & c_{12} c_{23} - s_{12} s_{23} s_{13} e^{i\delta} & s_{23} c_{13} \\ s_{12} s_{23} - c_{12} c_{23} s_{13} e^{i\delta} & -c_{12} s_{23} - s_{12} c_{23} s_{13} e^{i\delta} & c_{23} c_{13} \end{pmatrix} \cdot V, \quad (7)$$

with

$$V = \text{diag}(e^{-i\frac{\phi_1}{2}}, e^{-i\frac{\phi_2}{2}}, 1), \quad (8)$$

where $c_{ij} \equiv \cos \theta_{ij}$, $s_{ij} \equiv \sin \theta_{ij}$. θ_{ij} are the neutrino flavour mixing angles, δ is the Dirac phase and $\phi_{1,2}$ are the Majorana phases.

In view of the above, the seesaw equation (4) can be solved for m_D as [23]

$$m_D = i\sqrt{m_N^{\text{diag}}} R \sqrt{m_\nu^{\text{diag}}} U_{\text{MNS}}^\dagger, \quad (9)$$

where R is a generic complex orthogonal 3×3 matrix that encodes the possible extra neutrino mixings (associated with the right-handed sector) in addition to the ones in U_{MNS} . R can be parameterised in terms of three complex angles, θ_i ($i = 1, 2, 3$) as [23]

$$R = \begin{pmatrix} c_2 c_3 & -c_1 s_3 - s_1 s_2 c_3 & s_1 s_3 - c_1 s_2 c_3 \\ c_2 s_3 & c_1 c_3 - s_1 s_2 s_3 & -s_1 c_3 - c_1 s_2 s_3 \\ s_2 & s_1 c_2 & c_1 c_2 \end{pmatrix}, \quad (10)$$

with $c_i \equiv \cos \theta_i$, $s_i \equiv \sin \theta_i$. Eq. (9) is a convenient means of parameterising our ignorance of the full neutrino Yukawa couplings, while at the same time allowing to accommodate the experimental data. Notice that it is only valid at the right-handed neutrino scales m_M , so that the quantities appearing in Eq. (9) are the renormalised ones, $m_\nu^{\text{diag}}(m_M)$ and $U_{\text{MNS}}(m_M)$.

We shall focus on the scenario where the light neutrinos are hierarchical, and we will assume a normal hierarchy,

$$m_{\nu_1} \ll m_{\nu_2} \ll m_{\nu_3}. \quad (11)$$

The masses $m_{\nu_{2,3}}$ can be written in terms of the lightest mass m_{ν_1} , and of the solar and atmospheric mass-squared differences as

$$\begin{aligned} m_{\nu_2}^2 &= \Delta m_{\text{sol}}^2 + m_{\nu_1}^2, \\ m_{\nu_3}^2 &= \Delta m_{\text{atm}}^2 + m_{\nu_1}^2. \end{aligned} \quad (12)$$

Regarding the heavy neutrinos, we will consider the two following cases,

$$\text{Degenerate: } m_{N_1} = m_{N_2} = m_{N_3} \equiv m_N ,$$

$$\text{Hierarchical: } m_{N_1} \ll m_{N_2} \ll m_{N_3} .$$

Concerning the SUSY parameters, and since we are working within an extended MSSM, with enlarged neutrino and sneutrino sectors, there will be new soft SUSY breaking parameters associated to the latter sectors. Thus, in addition to the usual soft breaking parameters for the gauginos ($M_{1,2,3}$), Higgs bosons ($M_{H_{1,2}}$), squarks ($m_{\tilde{Q}}, m_{\tilde{U}}, m_{\tilde{D}}, A_q$) and sleptons ($m_{\tilde{L}}, m_{\tilde{E}}, A_l$), there will also be the sneutrino soft breaking masses $m_{\tilde{M}}$, the sneutrino trilinear couplings A_ν , and the new bilinear parameter B_M . As already mentioned in the introduction, we will work in a constrained MSSM, where the number of input parameters is reduced by assuming partial universality of the soft parameters at the gauge coupling unification scale, $M_X = 2 \times 10^{16}$ GeV. Specifically, we will work in two scenarios, the CMSSM-seesaw with universal scalar masses, trilinear couplings and gaugino masses, and the NUHM-seesaw with non-universal soft masses for the Higgs bosons. Therefore, when specifying the parameters of these two constrained MSSM scenarios we will fix, in addition to the seesaw parameters, the following soft SUSY breaking parameters at the scale M_X :

$$\text{CMSSM-seesaw: } M_0, M_{1/2}, A_0, \tan \beta, \text{sign}(\mu) ,$$

$$\text{NUHM-seesaw: } M_0, M_{1/2}, A_0, \tan \beta, \text{sign}(\mu), M_{H_1}, M_{H_2} . \quad (13)$$

The departure from universality in the NUHM-seesaw will be parameterised in terms of the non-vanishing parameters δ_1 and δ_2 ,

$$\text{Non-universality: } M_{H_1}^2 = M_0^2 (1 + \delta_1), \quad M_{H_2}^2 = M_0^2 (1 + \delta_2) . \quad (14)$$

For simplicity, and to further reduce the number of input parameters, in this case we will also impose $M_0 = M_{1/2} \equiv M_{\text{SUSY}}$.

Once the above set of parameters is fixed at M_X , the predictions for the low-energy parameters are obtained by solving the full one-loop RGEs, including the extended neutrino and sneutrino sectors. Due to the existence of intermediate scales m_M introduced by the seesaw mechanism, the running must be carried out in two steps. The full set of equations is first run down from M_X to m_M . At the seesaw scales, the right-handed neutrinos as well as their SUSY partners decouple, and the new RGEs (without the equations and terms for ν_R and $\tilde{\nu}_R$) are then run down from m_M to the EW scale, where the couplings and mass matrices are finally computed.

Working in constrained MSSM scenarios, all flavour mixing originates solely from the neutrino Yukawa couplings, which induce flavour violation in the slepton sector by the RGE running from M_X down to the EW scale m_Z . Flavour mixing is then manifest in the values of the off-diagonal elements of the charged slepton squared mass matrix. The LL , RR , LR and RL elements of the latter $M_{\tilde{l}}^2$ matrix can be summarised as follows:

$$\begin{aligned}
M_{LL}^{ij2} &= m_{\tilde{L},ij}^2 + v_1^2 \left(Y_l^\dagger Y_l \right)_{ij} + m_Z^2 \cos 2\beta \left(-\frac{1}{2} + \sin^2 \theta_W \right) \delta_{ij}, \\
M_{RR}^{ij2} &= m_{\tilde{E},ij}^2 + v_1^2 \left(Y_l^\dagger Y_l \right)_{ij} - m_Z^2 \cos 2\beta \sin^2 \theta_W \delta_{ij}, \\
M_{LR}^{ij2} &= v_1 \left(A_l^{ij} \right)^* - \mu Y_l^{ij} v_2, \\
M_{RL}^{ij2} &= \left(M_{LR}^{ji2} \right)^*.
\end{aligned} \tag{15}$$

In the above, m_Z denotes the Z -boson mass, θ_W the weak mixing angle, and $i, j = 1, 2, 3$ are flavour indices. Given that below m_M the right-handed sneutrinos decouple, the low-energy sneutrino mass eigenstates are dominated by the $\tilde{\nu}_L$ components. Thus, sneutrino flavour mixing is confined to the left-handed sector, and described by the following 3×3 matrix:

$$M_{\tilde{\nu}}^{ij2} = m_{\tilde{L},ij}^2 + \frac{1}{2} m_Z^2 \cos 2\beta \delta_{ij}. \tag{16}$$

The physical masses and states are obtained by diagonalising the previous mass matrices, leading to

$$\begin{aligned}
M_{\tilde{l}}^{2\text{diag}} &= R^{(l)} M_{\tilde{l}}^2 R^{(l)\dagger} = \text{diag} (m_{\tilde{l}_1}^2, \dots, m_{\tilde{l}_6}^2), \\
M_{\tilde{\nu}}^{2\text{diag}} &= R^{(\nu)} M_{\tilde{\nu}}^2 R^{(\nu)\dagger} = \text{diag} (m_{\tilde{\nu}_1}^2, m_{\tilde{\nu}_2}^2, m_{\tilde{\nu}_3}^2),
\end{aligned} \tag{17}$$

where $R^{(l,\nu)}$ are unitary rotation matrices.

After having introduced our scenario, in the next section we will summarise some of the more relevant details leading to the computation of $\mu - e$ conversion rates in nuclei.

3 Analytical results of the $\mu - e$ conversion rates

In this section we report the analytical results for the $\mu - e$ conversion rates in terms of the parameters introduced in Section 2. We emphasise that all the results are obtained in terms of physical mass eigenstates (with full propagators) for all MSSM particles entering in the computation, namely, charginos $\tilde{\chi}_A^-(A = 1, 2)$, neutralinos $\tilde{\chi}_A^0(A = 1, \dots, 4)$, charged sleptons $\tilde{l}_X^-(X = 1, \dots, 6)$, sneutrinos $\tilde{\nu}_X^-(X = 1, 2, 3)$ and the neutral Higgs bosons, h^0 and H^0 .

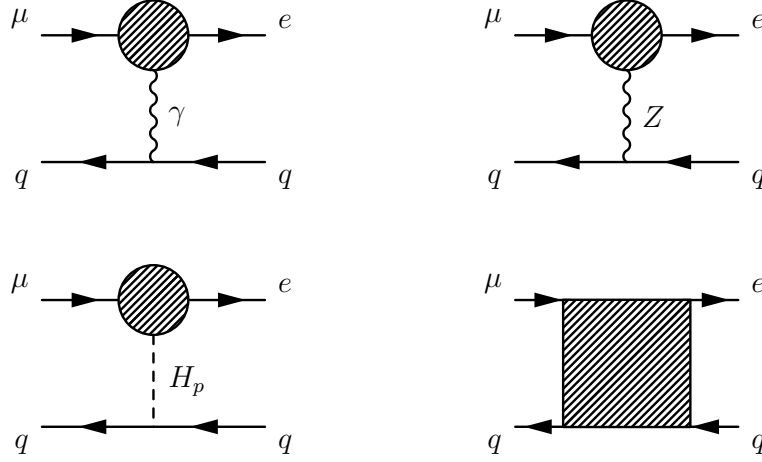


Figure 1: Photon-, Z -, H -penguin and box diagrams contributing to $\mu - e$ conversion in nuclei.

For the presentation of the results we closely follow the general parameterisation (and approximations) of [3]. One starts with the most general effective Lagrangian for four-fermion interactions which describes coherent $\mu - e$ conversion. At the quark level, this is given by

$$\mathcal{L}_{\text{eff}} = -\frac{G_F}{\sqrt{2}} \sum_q \left\{ [g_{LS(q)} \bar{e}_L \mu_R + g_{RS(q)} \bar{e}_R \mu_L] \bar{q} q + [g_{LV(q)} \bar{e}_L \gamma^\mu \mu_L + g_{RV(q)} \bar{e}_R \gamma^\mu \mu_R] \bar{q} \gamma_\mu q \right\}, \quad (18)$$

where G_F is the Fermi coupling. Notice that only scalar (S) and vector (V) effective operators do contribute, with couplings given by $g_{LS(q)}, g_{RS(q)}$ and $g_{LV(q)}, g_{RV(q)}$ (respectively left and right, in both cases). This effective Lagrangian at the quark level is then converted into an effective Lagrangian at the nucleon level, by means of the appropriate nucleon form factors [24]. In the limit of negligible momentum dependence of the nucleon form factors, (a reasonable approximation given the small momentum transfer in the $\mu - e$ process), the quark matrix elements can be simply replaced by the nucleon matrix elements as follows:

$$\begin{aligned} \langle p | \bar{q} \Gamma_K q | p \rangle &= G_K^{(q,p)} \bar{p} \Gamma_K p, \\ \langle n | \bar{q} \Gamma_K q | n \rangle &= G_K^{(q,n)} \bar{n} \Gamma_K n, \end{aligned} \quad (19)$$

where $\Gamma_K = (1, \gamma_\mu)$ respectively for $K = (S, V)$. The numerical values of the relevant G_K 's are [3, 25]:

$$\begin{aligned} G_V^{(u,p)} &= G_V^{(d,n)} = 2; & G_V^{(d,p)} &= G_V^{(u,n)} = 1; \\ G_S^{(u,p)} &= G_S^{(d,n)} = 5.1; & G_S^{(d,p)} &= G_S^{(u,n)} = 4.3; \\ G_S^{(s,p)} &= G_S^{(s,n)} = 2.5. \end{aligned} \quad (20)$$

The conversion rates are then predicted in terms of the relevant isoscalar, $g_{XK}^{(0)}$, and isovector couplings, $g_{XK}^{(1)}$ (with $X = L, R$ and $K = S, V$), which are given by:

$$\begin{aligned} g_{XK}^{(0)} &= \frac{1}{2} \sum_{q=u,d,s} \left(g_{XK(q)} G_K^{(q,p)} + g_{XK(q)} G_K^{(q,n)} \right), \\ g_{XK}^{(1)} &= \frac{1}{2} \sum_{q=u,d,s} \left(g_{XK(q)} G_K^{(q,p)} - g_{XK(q)} G_K^{(q,n)} \right). \end{aligned} \quad (21)$$

Further working under the approximation of equal proton and neutron densities in the nucleus, and of a non-relativistic muon wave function for the $1s$ state, the final formula for the $\mu - e$ conversion rate, relative to the muon capture rate, can be finally written as

$$\begin{aligned} \text{CR}(\mu - e, \text{Nucleus}) &= \frac{p_e E_e m_\mu^3 G_F^2 \alpha^3 Z_{\text{eff}}^4 F_p^2}{8 \pi^2 Z} \\ &\times \left\{ \left| (Z + N) \left(g_{LV}^{(0)} + g_{LS}^{(0)} \right) + (Z - N) \left(g_{LV}^{(1)} + g_{LS}^{(1)} \right) \right|^2 + \right. \\ &\quad \left. \left| (Z + N) \left(g_{RV}^{(0)} + g_{RS}^{(0)} \right) + (Z - N) \left(g_{RV}^{(1)} + g_{RS}^{(1)} \right) \right|^2 \right\} \frac{1}{\Gamma_{\text{capt}}}, \end{aligned} \quad (22)$$

where Z and N are the number of protons and neutrons in the nucleus, while Z_{eff} is an effective atomic charge, obtained by averaging the muon wave function over the nuclear density [26]. F_p is the nuclear matrix element and Γ_{capt} denotes the total muon capture rate. The other quantities in the above formula correspond to the muon mass, m_μ , the momentum and energy of the electron, p_e and E_e (which are set to m_μ in the numerical evaluation), and the electromagnetic coupling constant, α .

We have computed the full set of one-loop diagrams leading into the quantity $\text{CR}(\mu - e, \text{Nucleus})$: γ -penguins, Z - and Higgs-boson penguins and box diagrams. These are schematically drawn at the quark level in Fig. 1, and receive contributions from several diagrams, mediated by SUSY particles, which are collected in Appendix A. The analytical results of the computation are summarised in terms of the contributions of these diagrams to the vector and scalar couplings,

$$\begin{aligned} g_{LV(q)} &= g_{LV(q)}^\gamma + g_{LV(q)}^Z + g_{LV(q)}^B, \\ g_{LS(q)} &= g_{LS(q)}^H + g_{LV(q)}^B. \end{aligned} \quad (23)$$

In the above, the photon couplings $g_{LX(q)}^\gamma$, the Z -boson couplings $g_{LX(q)}^Z$, the H -boson couplings $g_{LS(q)}^H$, and the couplings arising from the boxes $g_{LX(q)}^B$ (with $X = V, S$) are respectively

given by

$$\begin{aligned}
g_{LV(q)}^\gamma &= \frac{\sqrt{2}}{G_F} e^2 Q (A_1^L - A_2^R) , \\
g_{LV(q)}^Z &= -\frac{\sqrt{2}}{G_F} \frac{Z_L^q + Z_R^q}{2} \frac{F_L}{m_Z^2} , \\
g_{LV(q)}^B &= -\frac{\sqrt{2}}{G_F} (B_q^{(n)LV} + B_q^{(c)LV}) , \\
g_{LS(q)}^H &= -\frac{\sqrt{2}}{G_F} \frac{1}{2} \sum_p \frac{1}{m_{H_p}^2} H_L^{(p)} (S_{L,q}^{(p)} + S_{R,q}^{(p)}) , \\
g_{LS(q)}^B &= -\frac{\sqrt{2}}{G_F} (B_q^{(n)LS} + B_q^{(c)LS}) .
\end{aligned} \tag{24}$$

Likewise, for the right-handed couplings we find

$$\begin{aligned}
g_{RV(q)} &= g_{LV(q)}|_{L \leftrightarrow R} , \\
g_{RS(q)} &= g_{LS(q)}|_{L \leftrightarrow R} .
\end{aligned} \tag{25}$$

The explicit formulae for the form factors of the photon ($A_{(1,2)}^{(L,R)}$), of the Z -boson ($F_{(L,R)}$), of the Higgs-boson ($H_{(L,R)}^{(p)}$, where $p = 1, 2, 3$ corresponds to $H_p = h^0, H^0, A^0$), and of the box diagrams ($B_q^{(n,c)(L,R)(V,S)}$) are listed in Appendix A. In each case, the relevant couplings $Z_{(L,R)}^q, S_{(L,R)q}^{(p)}$ etc., can be found in Appendix B.

It is important to stress that $S_{L,q}^{(3)} + S_{R,q}^{(3)}$ vanishes and therefore there are no contributions from the CP-odd Higgs boson A^0 . This is a consequence of working in the approximation of coherent $\mu - e$ conversion, in which case the initial and final nucleus state is the same, thus leading to vanishing matrix elements for pseudoscalar currents like $\langle \text{Nucleus} | \bar{q} \gamma_5 q | \text{Nucleus} \rangle$. Also notice that from the values of the $S_{(L,R)q}^{(p)}$ Higgs couplings, one can anticipate that in the large $\tan \beta$ and small Higgs mass regime, the dominant Higgs contribution will be that of H^0 .

When compared to the results obtained in [16], our expressions coincide in the formulae for the photon-penguins. Up to a global sign, the vector contributions from boxes also agree. Divergences occur regarding the Z -penguins, and the differences can be read by comparing our expressions in Eqs. (44-48) of Appendix A, with those of Eqs.(22-29) in [16]. As previously mentioned, we have included in addition scalar contributions from boxes and Higgs-mediated diagrams not considered in [16].

A connection between our results for the Higgs contributions and those reported in [17] can be established in the large $\tan \beta$ limit, writing the output in the mass-insertion approximation format. Under these conditions, and considering the limit of a common mass for all

SUSY particles involved, which is much larger than the SM particle masses, $M_{\text{soft}} \sim \mu \sim M_{\text{SUSY}} \gg m_W$, one arrives at the following simple expression for the dominant H^0 form factor [27]

$$H_L^{(2)} = -\frac{1}{(4\pi)^2} \frac{m_\mu}{12 m_W} \delta_{21}^l \tan^2 \beta \left[1 + \frac{1}{2}(1 - 3 \tan^2 \theta_W) \right], \quad (26)$$

where the first term arises from chargino mediated loops, while the second stems from neutralino mediated contributions. In the mass insertion approximation, the dominant slepton mixing effects are associated with δ_{21}^l , which can be written as:

$$\delta_{21}^l = \frac{(\Delta m_{\tilde{L}}^2)_{21}}{M_{\text{SUSY}}^2}. \quad (27)$$

From the above, one can finally obtain a simple expression for the H^0 contribution to the conversion rate, which is clearly dominated by the strange quark coupling, due to the enhancement in the coupling by m_s . This arises via $g_{LS}^{(0)} \simeq g_{LS(s)}^{H^0} G_S^{(s,p)}$ with

$$g_{LS(s)}^{H^0} = \frac{\sqrt{2}}{G_F} \frac{1}{2} \frac{1}{m_{H^0}^2} H_L^{(2)} \frac{g m_s}{m_W} \tan \beta. \quad (28)$$

Plugging this simplified result for the $g_{LS}^{(0)}$ coupling into the approximate conversion rate for the Higgs-dominated case,

$$\text{CR}(\mu - e, \text{Nucleus}) \simeq \frac{p_e E_e m_\mu^3 G_F^2 \alpha^3 Z_{\text{eff}}^4 F_p^2}{8\pi^2 Z} \left\{ \left| (Z + N) g_{LS}^{(0)} \right|^2 \right\} \frac{1}{\Gamma_{\text{capt}}} \quad (29)$$

we obtain the expected $\tan^6 \beta$ enhancement of the H^0 contribution. Moreover, the dependence on the Higgs mass ($\frac{1}{m_{H^0}^4}$), as well as the typical prefactor $|\delta_{21}^l|^2$ accounting for the lepton flavour changing effect are equally recovered. Within this approximation, and taking a specific value of $\delta_{21}^l = 10^{-3}$, allows to obtain an order-of-magnitude estimate for the conversion rate in the case of Titanium nuclei,

$$\text{CR}(\mu - e, \text{Ti}) \simeq \mathcal{O}(10^{-12}) \left(\frac{115 \text{ GeV}}{m_{H^0}} \right)^4 \left(\frac{\tan \beta}{50} \right)^6, \quad (30)$$

in agreement with the estimate of [17].

Finally, it is worth mentioning that the heavy SUSY particles do not decouple in the Higgs contributions to the $\mu - e$ conversion rates. This can be understood from the previous result of $H_L^{(2)}$ in Eq. (26), which is constant in the large M_{SUSY} limit. This SUSY non-decoupling effect has also been noticed in association to other Higgs-mediated LFV processes [27–30].

4 Numerical results and discussion

In this section we present the numerical results of the $\mu - e$ conversion rates in nuclei within the SUSY-seesaw context described in Section 2. We begin by addressing the CMSSM-seesaw, and then proceed to the NUHM-seesaw. In both scenarios, we consider the dependence of the theoretical predictions for the conversion rates on the most relevant SUSY-seesaw parameters. In our discussion, we will give a particular emphasis to the most significant differences between the CMSSM- and NUHM-seesaw scenarios.

The numerical results presented in this section are mainly devoted to the particular case of Titanium nuclei, given that one expects a notable improvement of future experimental sensitivities in that case [13]. However, some additional predictions for other nuclei are also included here, for comparison. The case of Gold nuclei is of particular interest, since at present the most stringent bound is that of $\text{CR}(\mu - e, \text{Au})$ [10].

For the purpose of numerical evaluation, we begin by defining the input parameters at the gauge coupling unification scale, M_X . In the case of a CMSSM-seesaw scenario, and instead of scanning over the full $(M_{1/2}, M_0, A_0, \tan\beta, \text{sign}\mu)$ parameter space, we study specific points, each exhibiting distinct characteristics from the low-energy phenomenology point of view. We specify these parameters by means of the “Snowmass Points and Slopes” (SPS) [31] cases defined in Table 1.

SPS	$M_{1/2}$ (GeV)	M_0 (GeV)	A_0 (GeV)	$\tan\beta$	μ
1 a	250	100	-100	10	> 0
1 b	400	200	0	30	> 0
2	300	1450	0	10	> 0
3	400	90	0	10	> 0
4	300	400	0	50	> 0
5	300	150	-1000	5	> 0

Table 1: Values of $M_{1/2}$, M_0 , A_0 , $\tan\beta$, and $\text{sign}\mu$ for the SPS points considered in the analysis.

In the case of the NUHM-seesaw scenario, and in order to reduce the number of input parameters, we set $M_0 = M_{1/2} \equiv M_{\text{SUSY}}$, and explore the $(M_{\text{SUSY}}, A_0, \tan\beta, \text{sign}\mu, \delta_1, \delta_2)$

parameter space considering the following intervals:

$$\begin{aligned}
250 \text{ GeV} &< M_{\text{SUSY}} < 1000 \text{ GeV}, \\
-500 \text{ GeV} &< A_0 < 500 \text{ GeV}, \\
5 &< \tan \beta < 50, \\
-2 &< \delta_1, \delta_2 < 2.
\end{aligned} \tag{31}$$

In addition, we also consider the two possibilities, $\text{sign}(\mu) = \pm 1$.

To obtain the low-energy parameters of the model (and thus compute the relevant physical masses and couplings), the full one-loop RGEs (including the neutrino and sneutrino sectors) are firstly run down from M_X to the right handed neutrino scale m_M . At this scale we impose the boundary condition of Eq. (9). After the decoupling of the heavy neutrinos and sneutrinos, the new RGEs are then run down from m_M to the EW scale, at which the conversion rates are computed. Notice that, in the case of hierarchical heavy neutrinos, the sequential running is done from M_X down to m_{N_3} and from m_{N_1} down to the EW scale. This implies that we do not take into account the running effects from the intermediate right handed neutrino scales, i.e. from m_{N_3} to m_{N_2} and from m_{N_2} to m_{N_1} . We have estimated these threshold effects by means of the leading logarithmic (LLog) approximation, verifying that they are indeed negligible for the numerical values chosen in the present work.

The numerical implementation of the above procedure is achieved by means of the public Fortran code **SPheno2.2.2** [32]. The value of M_X is derived from the unification condition of the $SU(2)$ and $U(1)$ gauge couplings (systematically leading to a value of M_X very close to 2×10^{16} GeV throughout the numerical analysis), while $|\mu|$ is derived from the requirement of obtaining the correct radiative EW symmetry breaking. The code **SPheno2.2.2** has been adapted [33] in order to fully incorporate the right-handed neutrino (and sneutrino) sectors, as well as the full lepton flavour structure. The computation of the $\mu - e$ conversion rates in nuclei, as well as of other LFV observables, has been implemented into the code by means of additional subroutines.

Regarding the light neutrino masses and the U_{MNS} matrix elements, we take the following input values:

$$\begin{aligned}
\Delta m_{\text{sol}}^2 &= 8 \times 10^{-5} \text{ eV}^2, \quad \Delta m_{\text{atm}}^2 = 2.5 \times 10^{-3} \text{ eV}^2, \quad m_{\nu_1} = 10^{-3} \text{ eV}, \\
\theta_{12} &= 30^\circ, \quad \theta_{23} = 45^\circ, \quad \theta_{13} \lesssim 10^\circ, \quad \delta = \phi_1 = \phi_2 = 0,
\end{aligned} \tag{32}$$

compatible with present experimental data (see, for instance, the analyses of [18]). We do not address the impact of non-vanishing U_{MNS} phases (Dirac or Majorana) in the $\mu - e$ conversion rates.

Finally, although not used in this work, it is clarifying to recall that a simplified estimation of the generated flavour mixing in the slepton sector can be obtained by means of the LLog approximation. Using the latter, the relevant off-diagonal slepton mass matrix element for the processes involving lepton flavour violation in the $\mu - e$ sector (as is the case of $\mu - e$ conversion in nuclei) can be given as

$$(\Delta m_L^2)_{21} = -\frac{1}{8\pi^2} (3M_0^2 + A_0^2) (Y_\nu^\dagger L Y_\nu)_{21} ; L_{kl} \equiv \log \left(\frac{M_X}{m_{N_k}} \right) \delta_{kl} . \quad (33)$$

Writing $(Y_\nu^\dagger L Y_\nu)_{21}$ using the parameterisation of Eqs. (5-10), and considering the limit of $m_{\nu_1} = 0$, $\phi_{1,2} = \delta = 0$ (which is appropriate for the subsequent discussion), one obtains the following expression:

$$\begin{aligned} v_2^2 (Y_\nu^\dagger L Y_\nu)_{21} = & L_{33} m_{N_3} [c_{13} \sqrt{m_{\nu_2}} c_2^* s_1^* s_{12} + \sqrt{m_{\nu_3}} c_1^* c_2^* s_{13}] \\ & [\sqrt{m_{\nu_3}} c_1 c_2 c_{13} s_{23} + \sqrt{m_{\nu_2}} c_2 s_1 (c_{12} c_{23} - s_{12} s_{13} s_{23})] \\ + L_{22} m_{N_2} [& \sqrt{m_{\nu_2}} c_{13} (c_1^* c_3^* - s_1^* s_2^* s_3^*) s_{12} - \sqrt{m_{\nu_3}} (c_3^* s_1^* + c_1^* s_2^* s_3^*) s_{13}] \\ & [-\sqrt{m_{\nu_3}} c_{13} (c_3 s_1 + c_1 s_2 s_3) s_{23} + \sqrt{m_{\nu_2}} (c_1 c_3 - s_1 s_2 s_3) (c_{12} c_{23} - s_{12} s_{13} s_{23})] \\ + L_{11} m_{N_1} [& -\sqrt{m_{\nu_2}} c_{13} (c_3^* s_1^* s_2^* + c_1^* s_3^*) s_{12} + \sqrt{m_{\nu_3}} (-c_1^* c_3^* s_2^* + s_1^* s_3^*) s_{13}] \\ & [\sqrt{m_{\nu_3}} c_{13} (-c_1 c_3 s_2 + s_1 s_3) s_{23} - \sqrt{m_{\nu_2}} (c_3 s_1 s_2 + c_1 s_3) (c_{12} c_{23} - s_{12} s_{13} s_{23})] . \end{aligned} \quad (34)$$

In what follows, we begin by investigating the theoretical predictions for the $\mu - e$ conversion rates in Titanium nuclei within the CMSSM-seesaw.

4.1 Universality: CMSSM-seesaw

The numerical results of the $\text{CR}(\mu - e, \text{Ti})$ within the CMSSM-seesaw scenario are displayed in figures 2 through 5. The following discussion is focused on the most relevant parameters, namely m_{N_i} , $\theta_{1,2,3}$, θ_{13} , $\tan \beta$, M_0 and $M_{1/2}$.

In Fig. 2, we display the prediction of $\text{CR}(\mu - e, \text{Ti})$ as a function of the heavy neutrino masses for the various SPS points, and for the particular choice $\theta_i = 0$ ($i = 1, 2, 3$) and $\theta_{13} = 5^\circ$. We also consider the case of degenerate and hierarchical heavy neutrino spectra (respectively left and right panels). In both scenarios for degenerate and hierarchical heavy neutrinos, we find a strong dependence on the heavy neutrino masses. We also see that the rates for the various SPS points exhibit the following hierarchy,

$\text{BR}_4 > \text{BR}_{1b} \gtrsim \text{BR}_{1a} > \text{BR}_3 \gtrsim \text{BR}_2 > \text{BR}_5$. This behaviour can be understood in terms of the growth of the CRs with $\tan\beta$, and from the different mass spectra associated with each point.

In the case of degenerate heavy neutrinos, we find the expected fast growing behaviour of $\text{CR}(\mu - e, \text{Ti})$ as a function of the common neutrino mass m_N . For the values of m_N within the studied interval $[10^9 \text{ GeV}, 10^{15} \text{ GeV}]$, the predictions for the $\text{CR}(\mu - e, \text{Ti})$ range over ten orders of magnitude. We also see that, for the chosen input parameter values, the predicted rates cross the experimental bound for the large m_N region. In the latter, the Yukawa couplings can be large (for instance, Y_{33}^ν and Y_{32}^ν can be $\mathcal{O}(1)$, while Y_{22}^ν and Y_{21}^ν can be of $\mathcal{O}(10^{-3})$), leading to excessively large rates, so that these large m_N values are disfavoured by data. The experimental bound is saturated for m_N values ranging from $2 \times 10^{13} \text{ GeV}$ for SPS 4 up to about 10^{15} GeV for SPS 5. In the case of hierarchical heavy neutrinos a similar behaviour of the predicted rates is found with respect to the heaviest neutrino mass, m_{N_3} . We have also checked that the conversion rates do not significantly depend on m_{N_1} and m_{N_2} , provided that their values are kept well below m_{N_3} . With the planned future sensitivity of 10^{-18} it will be possible to reach into wider regions of the heavy neutrino spectrum. Heavy neutrino masses above 10^{12} GeV can be probed for the several considered scenarios.

For most of the studied points, the previously illustrated dependence of the rates on the heavy neutrino masses is in agreement with the expected behaviour $|m_N \log m_N|^2$ obtained in the LLog approximation (as derived from Eq. (34)). However, a clear departure from this approximation is found for some points, the most remarkable being the case of SPS 5. This failure of the LLog approximation has been known to happen in some scenarios, for instance those with either large A_0 , or low M_0 and large $M_{1/2}$ [34].

The predictions for $\text{CR}(\mu - e, \text{Ti})$ as a function of the R -matrix angles, $\theta_{1,2,3}$, are displayed in Fig. 3. In this case we have fixed the other relevant parameters as $\theta_{13} = 5^\circ$, $m_N = 10^{13} \text{ GeV}$ and $m_{N_i} = (10^{10}, 10^{11}, 10^{13}) \text{ GeV}$ (degenerate and hierarchical heavy neutrinos, respectively) and chosen SPS 1a. To fully explore the variation of the rates with the complex angles¹ θ_i , we have scanned the intervals $0 < |\theta_i| < \pi \text{ rad}$ and $0 \leq \arg \theta_i \leq \frac{\pi}{2} \text{ rad}$. From this figure we see that the dependence on the three θ_i is very similar in the degenerate case, whereas the same does not occur for hierarchical heavy neutrinos. In the former, the rates smoothly grow

¹Complex θ_i may imply the presence of CP violation in the neutrino Yukawa couplings. In addition to affecting the LFV rates, these phases will induce contributions to flavour-conserving CP violating observables, as is the case of charged lepton electric dipole moments (EDMs). Throughout the present study we have verified that the associated predictions for the charged lepton EDMs are in agreement with current experimental bounds [2].

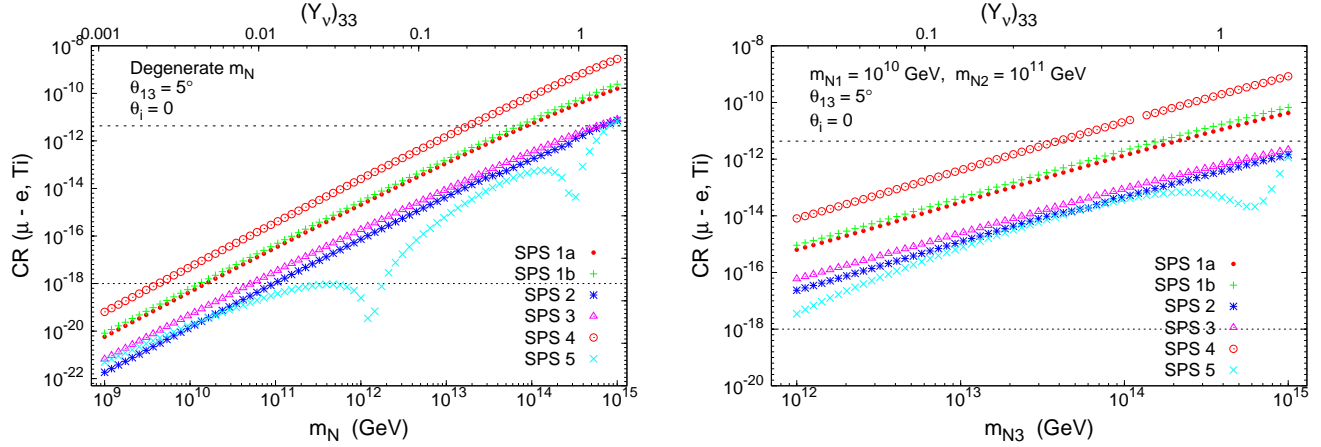


Figure 2: $\text{CR}(\mu - e, \text{Ti})$ as a function of the relevant heavy neutrino mass: m_N (on the left) and m_{N_3} (on the right), respectively associated with the degenerate and hierarchical cases. The predictions for SPS 1a (dots), 1b (crosses), 2 (asterisks), 3 (triangles), 4 (circles) and 5 (times) are included. On the upper horizontal axis we display the associated value of $(Y_\nu)_{33}$. In each case, we set $\theta_{13} = 5^\circ$, and consider the limit where $R = 1$ ($\theta_i = 0$). A dashed (dotted) horizontal line denotes the present experimental bound (future sensitivity).

with both modulus and argument, and are independent of θ_i in the real case. In the latter, the rates are almost independent of θ_3 , and present a different minima pattern regarding θ_1 and θ_2 . The deep minima occurring in the real case are a consequence of the corresponding minima appearing in the relevant elements of the Yukawa couplings (as given by Eq. (9)). Notice that the observed behaviour of $\text{CR}(\mu - e, \text{Ti})$ as a function of θ_i can be indeed easily understood from the simple analytical expression obtained in the LLog approximation (cf. Eq. (34)).

The most important outcome from Fig. 3 is that for both cases of degenerate and hierarchical heavy neutrinos, complex values of θ_i can increase the $\mu - e$ conversion rates by almost five orders of magnitude with respect to the $\theta_i = 0$ case. Only for a few specific choices of θ_i (for instance real θ_1 or θ_2 , in the hierarchical case) can we observe a strong decrease with respect to the $\theta_i = 0$ case, but clearly this is not a generic situation.

In the following, and in order to simplify the analysis with respect to the other parameters, we will set $\theta_i = 0$, and assume that the corresponding predictions for the $\text{CR}(\mu - e, \text{Ti})$ will constitute a representative case for the lowest conversion rates.

In Fig. 4 we show the dependence of the $\mu - e$ conversion rates on the light neutrino mixing angle θ_{13} . The other parameters are set to $m_N = 10^{14}$ GeV, $m_{N_i} = (10^{10}, 10^{11}, 10^{14})$ GeV, (respectively for degenerate and hierarchical heavy neutrinos) and $\theta_i = 0$. All the SPS

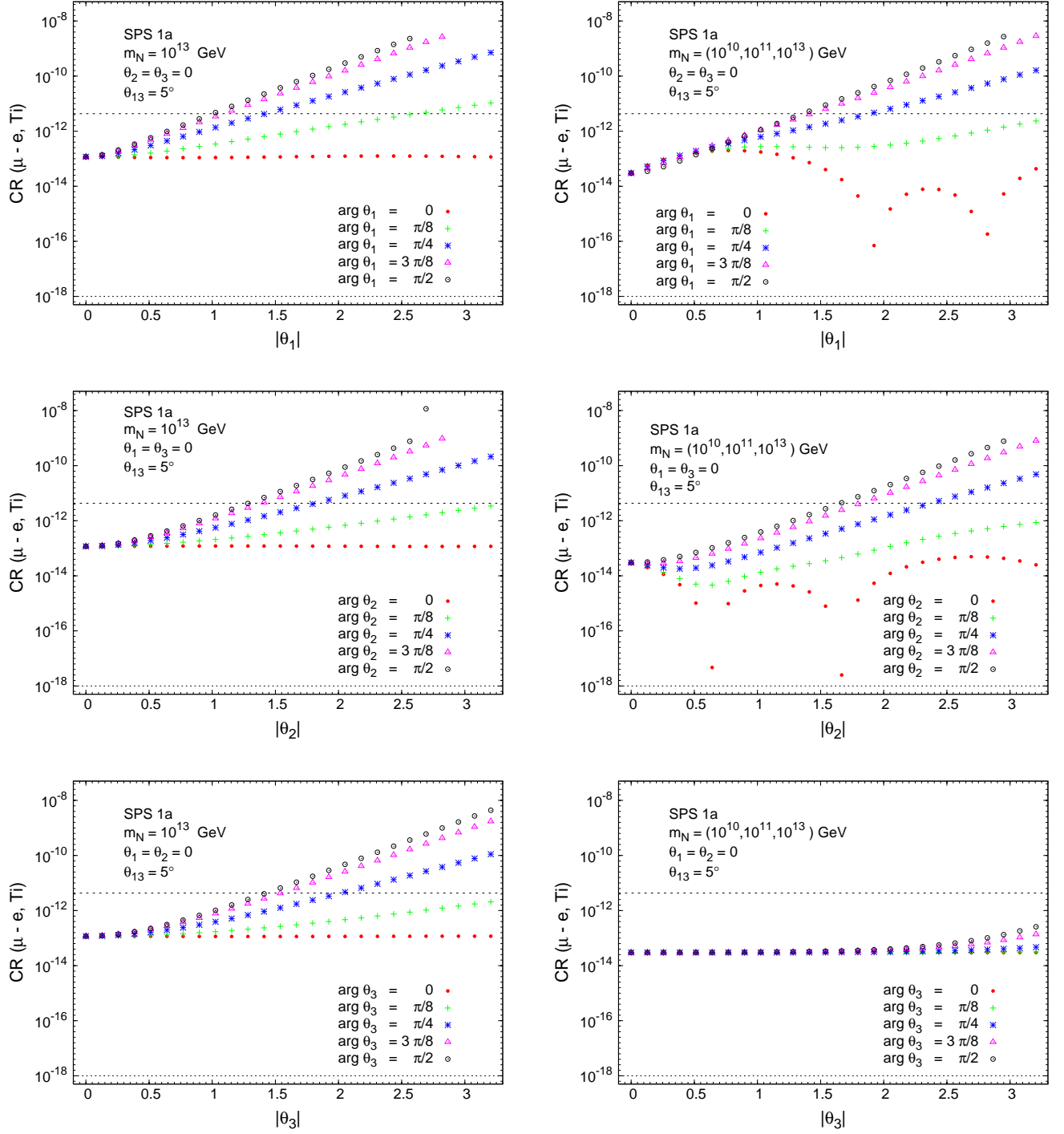


Figure 3: From top to bottom, $\text{CR}(\mu - e, \text{Ti})$ as a function of $|\theta_i|$ ($i = 1, 2, 3$), for $\arg \theta_i = \{0, \pi/8, \pi/4, 3\pi/8, \pi/2\}$ (dots, crosses, asterisks, triangles and circles, respectively). Both $|\theta_i|$ and $\arg \theta_i$ are given in radians. On the left we consider degenerate heavy neutrinos (with $m_N = 10^{13}$ GeV), while on the right the hierarchical case is displayed (with $m_{N_i} = (10^{10}, 10^{11}, 10^{13})$ GeV). In all cases we take $\theta_{13} = 5^\circ$, and set the CMSSM parameters to the SPS 1a case. A dashed (dotted) horizontal line denotes the present experimental bound (future sensitivity).

points in Table 1 have been considered. For degenerate heavy neutrinos, the dependence on θ_{13} is softer than what is observed for the hierarchical case, leading to a variation in the

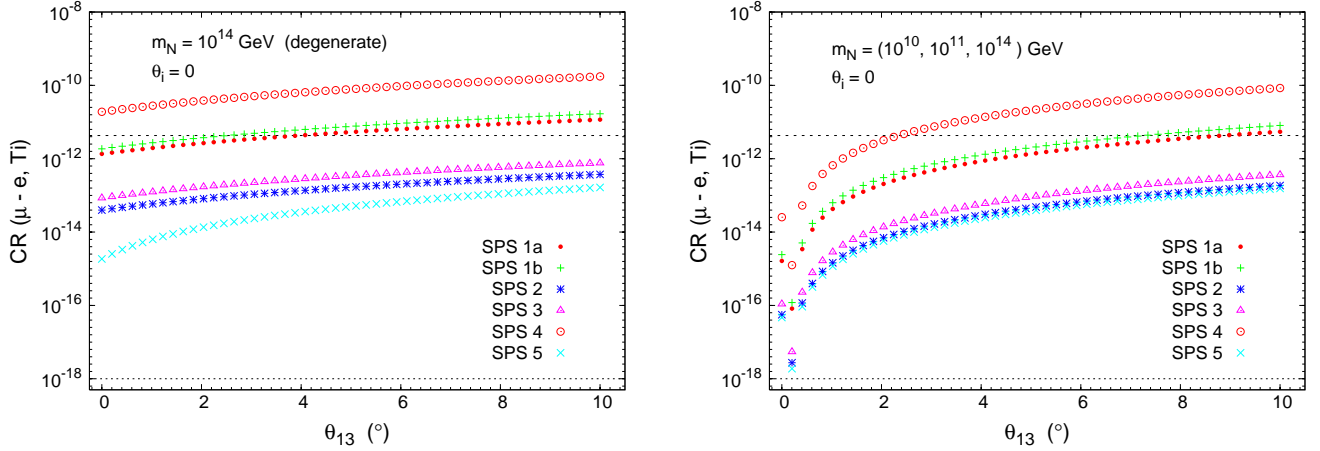


Figure 4: $\text{CR}(\mu - e, \text{Ti})$ as a function of θ_{13} (in degrees), for SPS 1a (dots), 1b (crosses), 2 (asterisks), 3 (triangles), 4 (circles) and 5 (times). On the left we consider degenerate heavy neutrinos (with $m_N = 10^{14}$ GeV), while on the right the hierarchical case is displayed (with $m_{N_i} = (10^{10}, 10^{11}, 10^{14})$ GeV). In both cases we choose $R = 1$ ($\theta_i = 0$). A dashed (dotted) horizontal line denotes the present experimental bound (future sensitivity).

rates of at most one order of magnitude in the studied range of $0^\circ \leq \theta_{13} \leq 10^\circ$ (the only exception being SPS 5, where the variation can reach up to two orders of magnitude). In contrast, this figure clearly manifests the very strong sensitivity of the $\text{CR}(\mu - e, \text{Ti})$ to the θ_{13} mixing angle for hierarchical heavy neutrinos. In the hierarchical case, a variation of θ_{13} in the studied interval leads to an increase in the conversion rates by as much as five orders of magnitude. This huge variation is due to the strong decrease of this observable for very small θ_{13} angles, as can be easily understood from the dependence on this angle of the dominant $(L_{33}m_{N_3}\sqrt{m_{\nu_3}}c_1^*c_2^*s_{13})$ term in Eq. (34). Furthermore, the minimum of $\text{CR}(\mu - e, \text{Ti})$ is expected to occur at a vanishing mixing angle, but this being the value at the seesaw scale, i.e., $\theta_{13}(m_M) = 0$. The deep minima in Fig. 4 are at $\theta_{13}(m_Z) \simeq 0.2^\circ$, which is precisely the RGE shifted value at m_Z from $\theta_{13}(m_M) = 0$. As θ_{13} grows, the predictions for SPS 4, SPS 1a and SPS 1b cross the present experimental bound. In particular, notice that for SPS 4, and for the present choice of input parameters, θ_{13} values larger than 2° would be excluded by present data.

An equally remarkable sensitivity to θ_{13} has been found in other $\mu - e$ violating processes, like $\mu \rightarrow e\gamma$ and $\mu \rightarrow 3e$, and also in tau decays as is the case of $\tau \rightarrow e\gamma$ and $\tau \rightarrow 3e$ [34]. This interesting behaviour with θ_{13} has been proposed in [34] as a powerful tool to test the seesaw-I hypothesis for neutrino mass generation and, in case of a measurement of these

branching ratios, as a unique way to derive some hints on the seesaw parameters, especially on the value of m_{N_3} . The $\mu - e$ conversion rates here presented will certainly add new interesting information on this type of analysis. Fig. 4 also shows that with the expected future sensitivity of 10^{-18} , the full $0^\circ \leq \theta_{13} \leq 10^\circ$ interval can be thoroughly covered.

In the following study we will restrict ourselves to the hierarchical case where we have found this strong sensitivity to θ_{13} . For definiteness, we will also fix the heavy neutrino masses and θ_{13} to “reference” values of $m_{N_i} = (10^{10}, 10^{11}, 10^{14})$ GeV and $\theta_{13} = 5^\circ$.

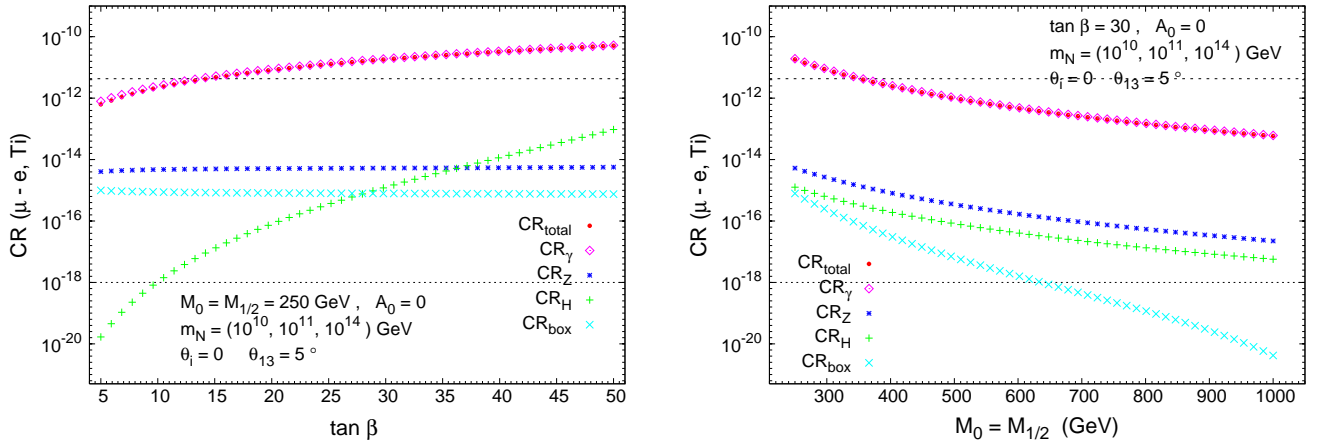


Figure 5: Contributions to $CR(\mu - e, Ti)$: total (dots), γ -penguins (diamonds), Z -penguins (asterisks), H -penguins (crosses) and box diagrams (times). On the left we present the dependence on $\tan\beta$, for $M_0 = M_{1/2} = 250$ GeV and $A_0 = 0$. On the right, we exhibit the evolution as a function of $M_0(= M_{1/2})$, for $\tan\beta = 30$ and $A_0 = 0$. In either case, we consider hierarchical heavy neutrinos with $m_{N_i} = (10^{10}, 10^{11}, 10^{14})$ GeV, and set $\theta_{13} = 5^\circ$, and $R = 1$ ($\theta_i = 0$). A dashed (dotted) horizontal line denotes the present experimental bound (future sensitivity).

Fig. 5 illustrates the predictions for the $CR(\mu - e, Ti)$ as a function of $\tan\beta$, M_0 and $M_{1/2}$. Here we have separately displayed the various contributions to the $\mu - e$ conversion rates in order to conclude about their relative importance in this CMSSM-seesaw scenario. We set the values of the remaining CMSSM parameters to $M_0 = M_{1/2} = 250$ GeV in the study with $\tan\beta$ (left panel) and to $\tan\beta = 30$ in the study with $M_{\text{SUSY}} \equiv M_0 = M_{1/2}$ (right panel), taking $A_0 = 0$ in both cases. We choose our “reference” values of $m_{N_{1,2,3}} = (10^{10}, 10^{11}, 10^{14})$ GeV, $\theta_{13} = 5^\circ$, and $\theta_i = 0$.

In both panels of Fig. 5 we clearly observe the dominance of the photon-mediated contributions, which are in fact indistinguishable from the total CR, for all the explored parameter ranges. The dependence of the various contributions on $\tan\beta$ illustrates the expected fast

growing behaviour with $\tan^6 \beta$ of the Higgs-mediated contributions, and the milder $\tan^2 \beta$ dependence of the photon-mediated ones. In addition, we see that the Z boson-mediated and the box diagram contributions are almost independent of $\tan \beta$. Although not displayed in this plot, we have also verified that the Higgs-mediated contribution is largely dominated by the exchange of H^0 , which is indeed the Higgs boson with enhanced couplings to charged leptons in the large $\tan \beta$ regime.

The decoupling behaviour for large M_{SUSY} of each of these contributions (CR_γ , CR_Z , CR_H and CR_{box}) is clearly manifested in the right panel of Fig. 5. The most important conclusion from this figure is that, within a CMSSM-seesaw scenario, the γ -penguin diagrams completely dominate the conversion rates, even for the largest $\tan \beta$ considered ($\tan \beta = 50$). Therefore, the total $\text{CR}(\mu - e, \text{Ti})$ does not manifest the Higgs contributions, so that in this universal scenario there is no chance for the $\mu - e$ conversion process to provide any information on the Higgs sector. We will see next that the situation is remarkably different in the non-universal case, where the Higgs contributions turn out to be much larger than in the universal case.

4.2 Non-universality: NUHM-seesaw

The numerical results for the NUHM-seesaw scenario are collected in figures 6 through 11.

In order to study the influence of the hypothesis of non-universal Higgs soft SUSY breaking masses, $M_{H_{1,2}}$, on the $\mu - e$ conversion rates, we have first explored the impact of the non-universality parameters δ_1 and δ_2 on the predicted Higgs boson masses. The values for these parameters have been taken to lie within the interval $-2 \leq \delta_{1,2} \leq 2$.

The predictions for the relevant Higgs boson mass, m_{H^0} , as a function of δ_1 and δ_2 are summarised in Fig. 6. We have chosen here the largest value of $\tan \beta = 50$ and three representative values of $M_{\text{SUSY}} = 250, 500$ and 850 GeV for moderate, heavy and very heavy SUSY spectra, respectively. The other parameters are set to our “reference” values of $m_{N_i} = (10^{10}, 10^{11}, 10^{14})$ GeV, $\theta_i = 0$, $A_0 = 0$, $\theta_{13} = 5^\circ$ and $\text{sign}(\mu) = +1$.

First, it is important to mention that not all the considered values of the $\delta_{1,2}$ parameters and M_{SUSY} allow for a correct $SU(2) \times U(1)$ breaking. In fact some particular choices for δ_1 , δ_2 , and M_{SUSY} lead to unacceptable negative values of $B\mu$ (and hence, negative $m_{A^0}^2$). For instance, this is the case when $\delta_{1,2}$ are simultaneously positive or negative. Some other points, despite leading to a proper $SU(2) \times U(1)$ breaking, are nevertheless not acceptable, since they lead to a Higgs boson sector which is too light, with masses below the present

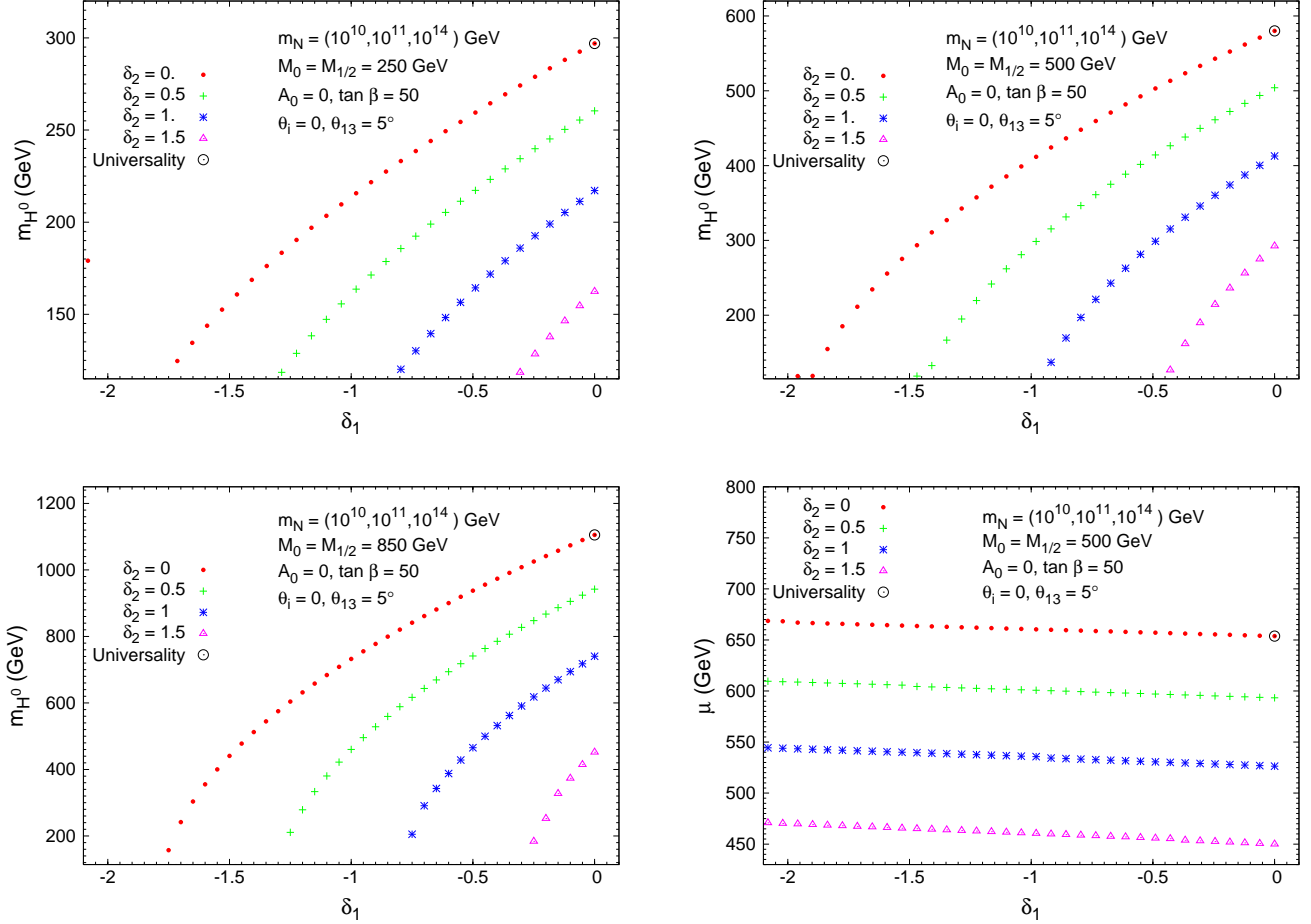


Figure 6: Mass of the heaviest Higgs scalar (m_{H^0}) as a function of the non-universality parameter δ_1 , for fixed values of $\delta_2 = \{0, 0.5, 1, 1.5\}$ (respectively dots, crosses, asterisks, triangles). The universality case $\delta_{1,2} = 0$ is represented by a large circle. We also take $m_{N_i} = (10^{10}, 10^{11}, 10^{14})$ GeV, set $\theta_i = 0$, $A_0 = 0$, $\tan \beta = 50$ and impose the relation $M_0 = M_{1/2}$. The first three plots correspond to $M_0 = 250, 500$ and 850 GeV, respectively. On the fourth plot, we display the μ parameter as a function of the non-universality parameter δ_1 , for fixed values of δ_2 , and for $M_0 = M_{1/2} = 500$ GeV.

experimental lower limits. To ensure that our results are indeed experimentally viable, we have included in this, and in the following figures, only the solutions where the three neutral Higgs boson masses are above the experimental bound for the lightest MSSM Higgs boson, which at present is 110 GeV for $\tan \beta > 5$ (99.7% C.L.) [2]. The most interesting solutions with important phenomenological implications are found for negative δ_1 and positive δ_2 , the choice selected for Fig. 6. In this figure, for all the explored values of δ_1 and δ_2 , we find a value of m_{H^0} that is significantly smaller than what one would encounter in the universal

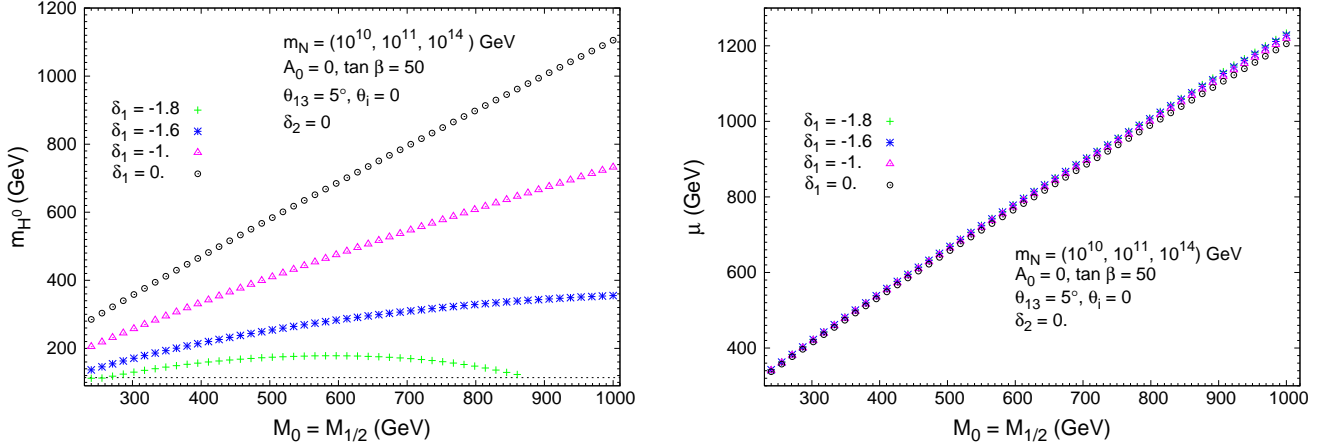


Figure 7: On the left, mass of the heaviest Higgs scalar (m_{H^0}) as a function of the SUSY scale ($M_{\text{SUSY}} = M_0 = M_{1/2}$), for fixed values of $\delta_1 = \{-1.8, -1.6, -1, 0\}$ (respectively crosses, asterisks, triangles and circles). We take $m_{N_i} = (10^{10}, 10^{11}, 10^{14})$ GeV, and set $\theta_i = 0$, $A_0 = 0$, $\tan \beta = 50$ with $\theta_{13} = 5^\circ$. On the right, the μ -parameter is displayed as a function of M_{SUSY} , for the same choices of SUSY-seesaw parameters.

case (here represented by the choice $\delta_1 = \delta_2 = 0$). This is truly remarkable in the case of large soft breaking masses, as can be seen, for instance, in the panel with $M_{\text{SUSY}} = 850$ GeV, where low values of m_{H^0} are still found, even close to the experimental limit. For completeness we have also shown in Fig. 6 the predictions for the μ parameter as a function of δ_1 and δ_2 . This parameter turns out to be nearly independent of δ_1 , and its largest values are obtained for $\delta_2 = 0$.

The behaviour of the predicted m_{H^0} and μ parameter as a function of $M_{\text{SUSY}} = M_0 = M_{1/2}$ is shown in Fig. 7. Here the specific values of $\delta_1 = \{-1.8, -1.6, -1, 0\}$ and $\delta_2 = 0$ have been considered. This figure again illustrates the interesting departure from the linear behaviour of m_{H^0} with M_{SUSY} , which is generic in the universal case ($\delta_{1,2} = 0$). In contrast, the μ parameter conserves a similar linear behaviour with M_{SUSY} in all the studied scenarios (universal and non-universal).

As a representative example of these interesting non-universal points, we explicitly refer to the case with $\delta_1 = -1.8$ and $\delta_2 = 0$, where the predicted masses are $m_{H^0} = 113, 174$ and 127 GeV for $M_{\text{SUSY}} = 250, 500$ and 850 GeV, respectively. For completeness, we have also collected the corresponding masses of the other relevant SUSY particles in Table 2. Notice that, in the case of $M_{\text{SUSY}} = 850$ GeV, this table illustrates a very heavy SUSY spectrum, even with a considerably heavy lightest SUSY particle, $m_{\tilde{\chi}_1^0} = 362$ GeV, but where the relevant Higgs boson is still light, $m_{H^0} = 127$ GeV.

MSSM masses (GeV)	M_{SUSY} (GeV)		
	250	500	850
$m_{\tilde{l}_1}$	175	415	734
$m_{\tilde{l}_2}$	258	511	867
$m_{\tilde{l}_3}$	258	511	867
$m_{\tilde{l}_4}$	307	594	985
$m_{\tilde{l}_5}$	309	607	1025
$m_{\tilde{l}_6}$	323	609	1031
$m_{\tilde{\nu}_1}$	281	571	971
$m_{\tilde{\nu}_2}$	297	601	1022
$m_{\tilde{\nu}_3}$	299	605	1028
$m_{\tilde{\chi}_1^-}$	185	395	687
$m_{\tilde{\chi}_2^-}$	379	679	1075
$m_{\tilde{\chi}_1^0}$	99	207	362
$m_{\tilde{\chi}_2^0}$	185	394	687
$m_{\tilde{\chi}_3^0}$	363	668	1067
$m_{\tilde{\chi}_4^0}$	377	678	1074
m_{h^0}	110	119	123
m_{H^0}	113	174	127

Table 2: Relevant MSSM spectra for $M_0 = M_{1/2} = M_{\text{SUSY}}$, $\tan\beta = 50$, $A_0 = 0$, $\theta_i = 0$, $\theta_{13} = 5^\circ$, $M_{N_i} = (10^{10}, 10^{11}, 10^{14})$ GeV, $\delta_1 = -1.8$ and $\delta_2 = 0$.

In the following we present the predictions of the $\mu - e$ conversion rates in Titanium nuclei within the NUHM-seesaw scenario. First we display in Fig. 8 the $\text{CR}(\mu - e, \text{Ti})$ as a function of $M_0 = M_{1/2} = M_{\text{SUSY}}$ and of A_0 for the particular choice $\delta_1 = -1.8$ and $\delta_2 = 0$. In order to illustrate the impact of the non-universality hypothesis on the conversion rates, we have separately displayed in this plot the various contributions from the γ -, Z -, Higgs mediated penguins and box diagrams. We observe a very distinct behaviour with M_{SUSY} of the Higgs-mediated contributions when compared to what was found for the CMSSM (universal) case, shown in Fig. 5. In fact, for the choice of input parameters in this plot, the Higgs-mediated contribution can equal, or even exceed that of the photon, dominating the total conversion rate in the large M_{SUSY} region. Both photon- and Higgs-mediated contributions are similar around $M_{\text{SUSY}} = 700$ GeV. These larger Higgs contributions are the obvious consequence of the lighter Higgs boson mass values encountered in this region, as

previously illustrated in Figs. 6 and 7. The non-decoupling behaviour of the SUSY particles for the large M_{SUSY} regime can be seen in the Higgs contribution, and thus in the total rates for the Higgs-dominated case.

For completeness, we have also explored other choices of A_0 and $\text{sign}(\mu)$. The case of $\text{sign}(\mu) = -1$, whose numerical results are not presented here, does not evidence any interesting new feature. In fact, there is a much more reduced δ_1, δ_2 parameter space allowing for the correct $SU(2) \times U(1)$ breaking. In addition, for $\text{sign}(\mu) = -1$ we have not found solutions displaying as small values of m_{H^0} as in the case of $\text{sign}(\mu) = +1$. The predicted Higgs contributions to the conversion rates are correspondingly smaller, and therefore less interesting. Regarding A_0 , the right panel in Fig. 8 shows that all the contributions are essentially independent of the value of the universal trilinear coupling, so that our selected value, $A_0 = 0$, is in fact a good representative point.

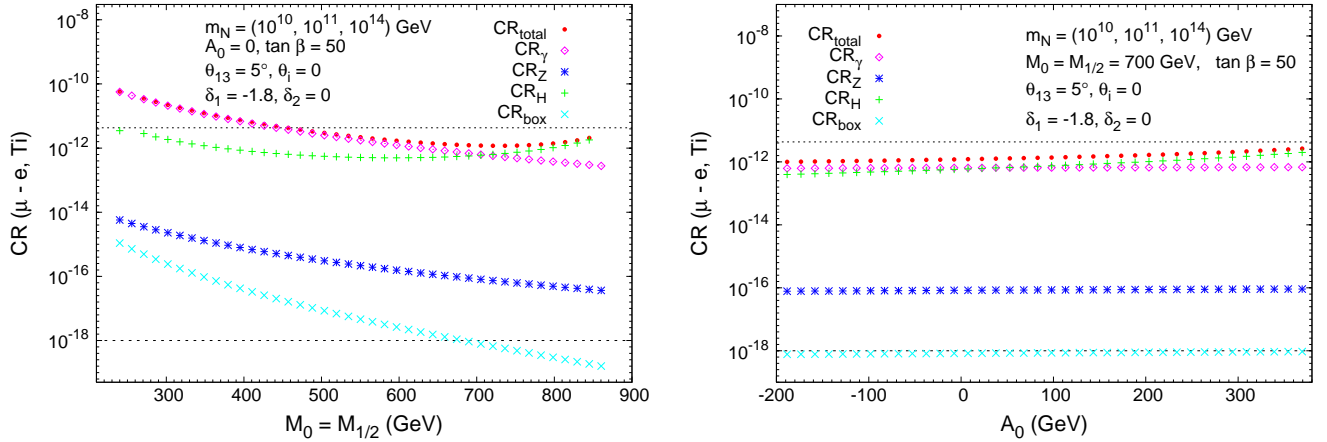


Figure 8: Contributions to $\text{CR}(\mu - e, \text{Ti})$ as a function of $M_0 (= M_{1/2})$ (left) and A_0 (right): total (dots), γ -penguins (diamonds), Z -penguins (asterisks), H -penguins (crosses) and box diagrams (times), for $\delta_1 = -1.8$ and $\delta_2 = 0$. We set $\tan \beta = 50$ and take $\theta_{13} = 5^\circ$, $R = 1$ ($\theta_i = 0$) and $m_{N_i} = (10^{10}, 10^{11}, 10^{14})$ GeV. On the left $A_0 = 0$, while on the right we choose $M_0 (= M_{1/2}) = 700$ GeV. In each case, a dashed (dotted) horizontal line denotes the present experimental bound (future sensitivity).

Within the NUHM-seesaw scenario, we have also studied the $\mu - e$ conversion rates for other nuclei. The case of Gold is particularly interesting since its present experimental bound of 7×10^{-13} [10] is more stringent than the present bound for Titanium (4.3×10^{-12} [9]). In Fig. 9 we display the predicted $\mu - e$ conversion rates for Al, Ti, Sr, Sb, Au and Pb, as a function of M_{SUSY} . We have chosen two light, two moderate and two heavy nuclei and we have fixed the other parameters to those of the previously elected non-universality reference

point (with $\delta_1 = -1.8$ and $\delta_2 = 0$). For completeness, the values of the relevant parameters for these nuclei, Z_{eff} , F_p and Γ_{capture} , have been collected in Table 3 and follow [35]. In this figure we clearly see that throughout most of the explored M_{SUSY} interval, the relative conversion rates obey the hierarchy $\text{CR}(\mu - e, \text{Sb}) > \text{CR}(\mu - e, \text{Sr}) > \text{CR}(\mu - e, \text{Ti}) > \text{CR}(\mu - e, \text{Au}) > \text{CR}(\mu - e, \text{Pb}) > \text{CR}(\mu - e, \text{Al})$, in agreement with the generic results in [35]. We do not find a significant difference in the large M_{SUSY} region, where the Higgs-contribution dominates the ratios. The predicted rates for Ti, Au and Pb tend to converge whereas the corresponding curve for Al nuclei deviates slightly from the others at large M_{SUSY} , but we do not consider these differences among the predictions for the various nuclei to be relevant. The most important conclusion from Fig. 9 concerns the fact that we have found predictions for Gold nuclei which, for the input parameters in this plot, are clearly above its present experimental bound throughout the explored M_{SUSY} interval. However, it should be recalled that the formulae here used for these estimates come from approximations that may not properly work for the case of very heavy nuclei. These heavy nuclei deserve a more dedicated and refined study.

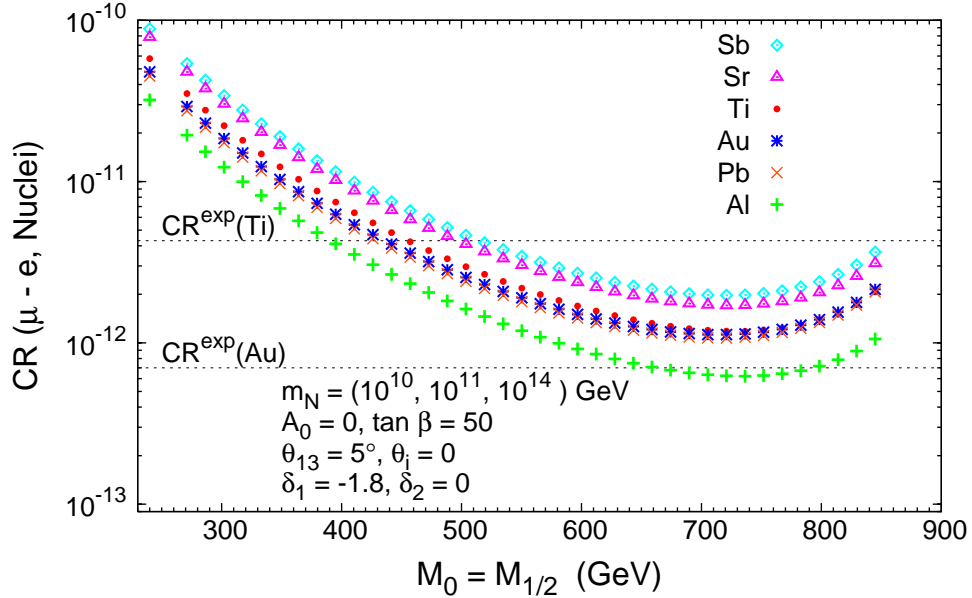


Figure 9: $\mu - e$ conversion rates for various nuclei as a function of $M_0 = M_{1/2}$ in the NUHM-seesaw. We display the theoretical predictions for Sb, Sr, Ti, Au, Pb and Al nuclei (diamonds, triangles, dots, asterisks, times and crosses, respectively). We have taken $m_{N_i} = (10^{10}, 10^{11}, 10^{14})$ GeV, $A_0 = 0$, $\tan \beta = 50$, $\theta_{13} = 5^\circ$ and $R = 1$ ($\theta_i = 0$). The non-universality parameters are set to $\delta_1 = -1.8$ and $\delta_2 = 0$. From top to bottom, the horizontal dashed lines denote the present experimental bounds for $\text{CR}(\mu - e, \text{Ti})$ and $\text{CR}(\mu - e, \text{Au})$.

${}^A_Z\text{Nucleus}$	Z_{eff}	F_p	$\Gamma_{\text{capt}}(\text{GeV})$
${}^{27}_{13}\text{Al}$	11.5	0.64	4.64079×10^{-19}
${}^{48}_{22}\text{Ti}$	17.6	0.54	1.70422×10^{-18}
${}^{80}_{38}\text{Sr}$	25.0	0.39	4.61842×10^{-18}
${}^{121}_{51}\text{Sb}$	29.0	0.32	6.71711×10^{-18}
${}^{197}_{79}\text{Au}$	33.5	0.16	8.59868×10^{-18}
${}^{207}_{82}\text{Pb}$	34.0	0.15	8.84868×10^{-18}

Table 3: Values of Z_{eff} , F_p and Γ_{capt} for different nuclei, as taken from [35].

Before proceeding with our analysis, let us briefly mention that for the region investigated in Fig. 9, the SUSY contributions to the anomalous magnetic moment of the muon, $a_\mu = (g_\mu - 2)$, range from $a_\mu^{\text{SUSY}} = 10^{-8}$ for $M_{\text{SUSY}} = 250$ GeV to $a_\mu^{\text{SUSY}} = 10^{-9}$, in association with $M_{\text{SUSY}} = 850$ GeV. The latter values are in fair agreement with the observed excess in a_μ^{exp} when compared to the SM prediction, which, at the 3.8σ is given by $a_\mu^{\text{SUSY}} = a_\mu^{\text{exp}} - a_\mu^{\text{SM}} = 3.32 \times 10^{-9}$ at 3.8σ (for a review, see for instance [36] and references therein).

To complete our study of the $\mu - e$ conversion rates in the NUHM-seesaw scenario we have compared the theoretical predictions for the $\text{CR}(\mu - e, \text{Ti})$ with those for the $\text{BR}(\mu \rightarrow e\gamma)$. We recall that both observables are sensitive to the same leptonic mixing given by the slepton mass matrix entries connecting the first and the second generation. In the usual photon-penguin dominated case, the latter two quantities are known to be highly correlated, and this is indeed what occurred for the CMSSM-seesaw discussed in Sec. 4.1. In other seesaw scenarios, as for instance, SUSY-GUT seesaw [37] or the inverse seesaw [38], this strong correlation still persists. However, for some scenarios where the photon-mediated diagrams are no longer the dominant contributions to the conversion rates, the strong correlation between $\text{CR}(\mu - e, \text{Ti})$ and $\text{BR}(\mu \rightarrow e\gamma)$ can be lost. For instance, this loss of correlation has been found in the case of Littlest Higgs Models, as recently pointed out in [39].

We have also found an interesting loss of correlation in the present case of the NUHM-scenario, where, as previously discussed, the Higgs-contributions can be the dominant ones. The departure from the strongly correlated regime for $(\text{CR}(\mu - e, \text{Ti}), \text{BR}(\mu \rightarrow e\gamma))$ is illustrated in Fig. 10, considering several choices of the neutrino mixing angle $\theta_{13} = 10^\circ, 5^\circ, 1^\circ, 0.2^\circ$. For all plots the predictions for $(\text{CR}(\mu - e, \text{Ti}), \text{BR}(\mu \rightarrow e\gamma))$ have been derived for several choices of the non-universality parameter δ_1 , scanning over the following interval $250 \text{ GeV} \leq M_{\text{SUSY}} \leq 1000 \text{ GeV}$. In each of the panels, the predictions for $(\text{CR}(\mu - e,$

Ti), $\text{BR}(\mu \rightarrow e\gamma)$) that correspond to $\delta_1 = \delta_2 = 0$ fall upon a straight line, which strongly supports the correlated behaviour of the two observables in this case. As M_{SUSY} increases within the considered interval, $(\text{CR}(\mu - e, \text{Ti}), \text{BR}(\mu \rightarrow e\gamma))$ moves left and downwards along the straight line due to the obvious decrease of the rate with M_{SUSY} .

However a clear departure from the previous strongly correlated predictions is found for other values of δ_1, δ_2 . In particular, for the specific δ_1 and δ_2 values where, as previously shown, the Higgs contributions dominate the $\mu - e$ conversion rates, the predicted $(\text{CR}(\mu - e, \text{Ti}), \text{BR}(\mu \rightarrow e\gamma))$ points exhibit a different behaviour, deviating from the straight line associated with the universal case. The separation between the correlated and uncorrelated regimes is maximal for the $\delta_1 = -1.8, \delta_2 = 0$ non-universal case, as can be clearly understood from our previous results. We find this loss of correlation a very promising phenomenon that could be fully explored if future sensitivities of 10^{-18} are reached.

Secondly, it is clear from Fig. 10 that even in the most pessimistic situation of very small θ_{13} , the theoretical predictions for $\text{CR}(\mu - e, \text{Ti})$, and in particular the corresponding curved line, are well above the horizontal line at 10^{-18} . This is quite a challenging possibility, since for those high values of $M_{\text{SUSY}} \sim 850$ GeV, whose predictions lie at the left end of the curved and straight lines, the predicted $\text{BR}(\mu \rightarrow e\gamma)$ is far below the planned 10^{-13} sensitivity. This clearly reflects that $\mu - e$ in nuclei can be a very competitive process to study LFV within the SUSY seesaw.

Finally, and to summarise the most striking results for these NUHM-seesaw scenarios, we plot in Fig. 11 the ratio of the two predicted rates, $\text{CR}(\mu - e, \text{Ti})/\text{BR}(\mu \rightarrow e\gamma)$ as a function of m_{H^0} . Since both observables exhibit the same dependence on m_{N_i}, θ_i and θ_{13} , the consideration of this ratio of rates allows to reduce the number of relevant parameters to $\tan\beta, M_{\text{SUSY}}$ and $\delta_{1,2}$. These last two are clearly the leading ones given that they drive the solutions to the interesting low m_{H^0} values. In this figure, and in order to maximise the Higgs-contribution to the total $\mu - e$ conversion rates we have again considered the extreme $\tan\beta = 50$ value. For consistency, we have set the remaining parameters to their reference values, but as we have said, they will not play a relevant role in this study.

Leading to this scatter plot, we have scanned in the intervals $-2 < \delta_1 < 0, 0 < \delta_2 < 2$ and $250 \text{ GeV} < M_{\text{SUSY}} < 1000 \text{ GeV}$. The most important conclusion from this plot is that the ratio $\text{CR}(\mu - e, \text{Ti})/\text{BR}(\mu \rightarrow e\gamma)$ can deviate from the constant prediction of 5×10^{-3} of the universality case by as much as a factor of almost 10. For the scan here conducted, the maximum value of this ratio of rates is found for $\delta_1 = -1.7, \delta_2 = 0.1$ and $M_{\text{SUSY}} = 876$ GeV, and its size is 0.04.

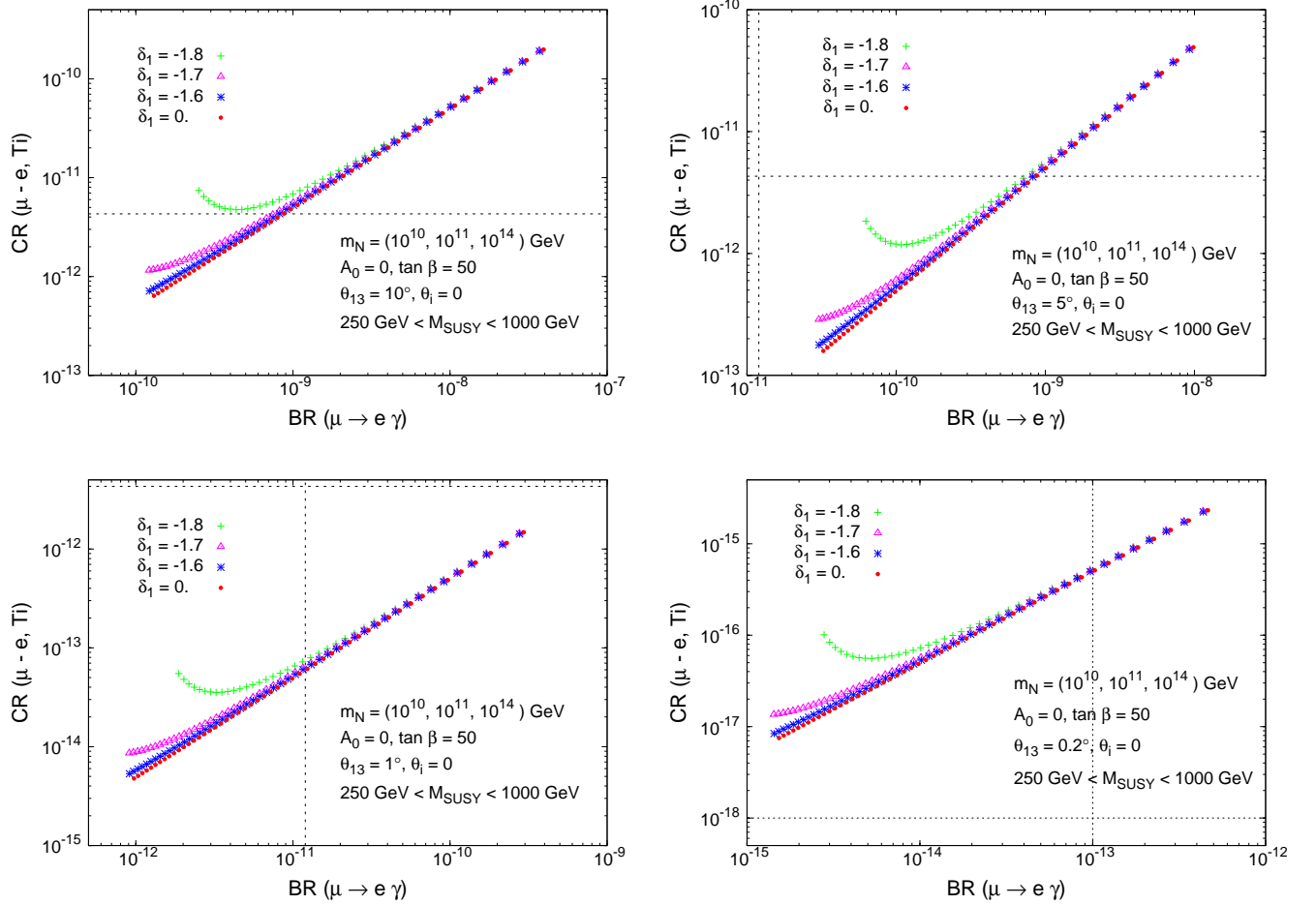


Figure 10: $\text{CR}(\mu - e, \text{Ti})$ versus $\text{BR}(\mu \rightarrow e \gamma)$ for $250 \text{ GeV} \leq M_{\text{SUSY}} \leq 1000 \text{ GeV}$, and $\delta_1 = -1.8, -1.7, -1.6, 0$ (crosses, triangles, asterisks, dots, respectively). We set $\delta_2 = 0$, and take $m_{N_i} = (10^{10}, 10^{11}, 10^{14}) \text{ GeV}$, $A_0 = 0$, $\tan \beta = 50$ and $R = 1$ ($\theta_i = 0$). From left to right and top to bottom, the panels are associated with $\theta_{13} = 10^\circ, 5^\circ, 1^\circ$ and 0.2° . In each case, the horizontal and vertical dashed (dotted) lines denote the present experimental bounds (future sensitivities) for $\text{CR}(\mu - e, \text{Ti})$ and $\text{BR}(\mu \rightarrow e \gamma)$, respectively.

Considering larger values of M_{SUSY} and identical intervals for $\delta_{1,2}$ leads to somewhat similar results: one finds the same pattern of clusters departing from the constant value of the universal case, but the maximum value of $\text{CR}(\mu - e, \text{Ti})/\text{BR}(\mu \rightarrow e \gamma)$ is in general smaller than the 0.04 obtained in the scan of Fig. 11. The reason why this ratio is not improved at larger values of M_{SUSY} than 1 TeV is because the acceptable solutions producing the proper $SU(2) \times U(1)$ breaking do not lead to sufficiently light Higgs bosons.

Even without the knowledge of the seesaw parameters, a measurement of $\text{CR}(\mu - e, \text{Ti})$

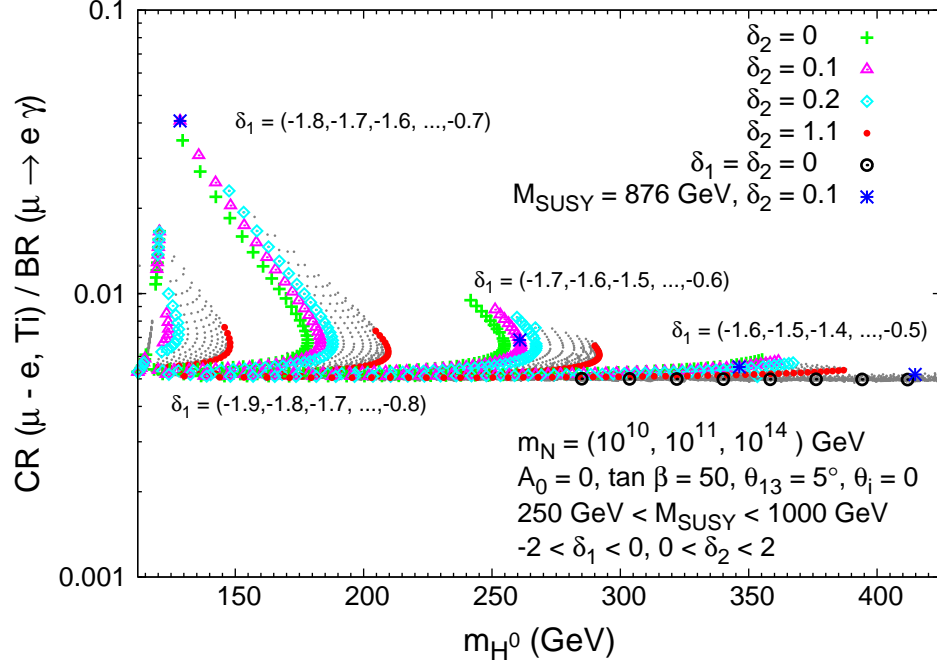


Figure 11: Ratio $\text{CR}(\mu - e, \text{Ti})/\text{BR}(\mu \rightarrow e\gamma)$ as a function of the Higgs mass, m_{H^0} . We take $m_{N_i} = (10^{10}, 10^{11}, 10^{14})$ GeV, $A_0 = 0$, $\tan \beta = 50$, $\theta_{13} = 5^\circ$ and $R = 1$ ($\theta_i = 0$), and scan over $250 \text{ GeV} \leq M_{\text{SUSY}} \leq 1000 \text{ GeV}$, $-2 \leq \delta_1 \leq 0$, and $0 \leq \delta_2 \leq 2$ (grey dots). We have highlighted specific choices of $\delta_2 = 0, 0.1, 0.2, 1.1$ (crosses, triangles, diamonds, dots, respectively). In each tilted cluster, we have also indicated the values of δ_1 associated with the δ_2 coloured points. The universality limit ($\delta_1 = \delta_2 = 0$) is denoted by a circle. Asterisks denote points with $M_{\text{SUSY}} = 876 \text{ GeV}$ and $\delta_2 = 0.1$.

and $\text{BR}(\mu \rightarrow e\gamma)$, together with information on $\tan \beta$ and the SUSY scale, may allow to shed some light into the Higgs sector.

5 Conclusions

In this work we have extensively studied the lepton flavour violating process of $\mu - e$ conversion in nuclei, within the context of the SUSY-seesaw. In particular, we considered two distinct scenarios, the CMSSM-seesaw, and the NUHM-seesaw, obtained by partially relaxing the universality conditions of the Higgs boson masses. Throughout our analysis, we compared our theoretical predictions with the present experimental bounds, and with the challenging future sensitivities. In fact, the latter may convert processes like $\text{CR}(\mu - e, \text{Ti})$ into one of the most sensitive probes to new physics.

We have presented here the first full one-loop computation of the $\mu - e$ conversion in

nuclei, including the complete set of SUSY-loop diagrams: γ -mediated, Z - and Higgs-boson mediated penguins and box diagrams. We have also provided the full analytical results working in terms of physical eigenstates (for all intervening SUSY and Higgs particles).

For the CMSSM-seesaw, we have considered the dependence of the conversion rates on the several parameters defining the scenario. Choosing the well known SPS benchmark points to specify the CMSSM parameters, we focused on the most relevant parameters in the neutrino sector, namely on the heavy neutrino masses (m_{N_i}), the complex θ_i mixing angles and the still undetermined angle of the U_{MNS} matrix, θ_{13} . As discussed here, the CRs exhibit a very pronounced dependence on the previous parameters, with variations that can reach up to ten orders of magnitude in the case of m_{N_i} and up to five orders of magnitude in the cases of θ_i and θ_{13} , for the investigated ranges. In turn, this strong dependence implies that a comparison of the theoretical predictions with the present experimental bound allows to derive indirect upper bounds for the unknown seesaw parameters.

We have pointed out that the highest sensitivity is found for the case of hierarchical heavy neutrinos. In this case, the conversion rates are essentially dependent on m_{N_3} and $\theta_{1,2}$, manifesting an extreme sensitivity to θ_{13} (for the case of vanishing θ_i). In fact, the values of these parameters in the upper part of their studied intervals, $10^{12} \text{ GeV} \leq m_{N_3} \leq 10^{15} \text{ GeV}$, $0 \leq |\theta_{1,2}| < \pi$, $0 \leq \arg(\theta_{1,2}) \leq \pi/2$ and $0^\circ \leq \theta_{13} \leq 10^\circ$ are already in conflict with the present upper bounds on $\text{CR}(\mu - e, \text{Ti})$ and $\text{CR}(\mu - e, \text{Au})$.

We have put special emphasis on the sensitivity of the $\text{CR}(\mu - e, \text{Ti})$ to θ_{13} , given that either a measurement, or a more stringent bound on this parameter is expected in the near future [40]. Therefore, and once θ_{13} is measured, a dedicated study of the $\mu - e$ conversion rates could provide some insight into the potentially unreachable heavy neutrino parameters.

In all the studied examples of the CMSSM-seesaw, the dominant contribution to the $\mu - e$ conversion rates clearly arises from the photon-penguins. Even though we have verified that the Higgs contributions do indeed grow with $\tan^6 \beta$, they induce contributions which are several orders of magnitude below those of the photon (which grow as $\tan^2 \beta$) for all the studied interval $5 \leq \tan \beta \leq 50$. A very interesting departure from this situation occurs when one relaxes the universality condition for the Higgs soft breaking masses, and this fuelled our interest to consider the NUHM-seesaw.

In the case of the NUHM-seesaw, we explored the influence of the non-universality hypothesis of the soft SUSY breaking masses $M_{H_{1,2}}$ on the $\mu - e$ conversion rates. The δ_1 and δ_2 parameters that describe the departure from universality in the Higgs sector have an important impact on the predicted Higgs boson masses. In particular, we have found regimes

for $\delta_{1,2}$ with very interesting phenomenological implications, namely the possibility of a light Higgs spectrum, even in the limit of large soft SUSY masses. As a concrete example, we recall that for the reference choice of $\delta_1 = -1.8$, $\delta_2 = 0$, we find $m_{H^0} = 113, 174$ and 127 GeV for $M_{\text{SUSY}} = 250, 500, 850$ GeV respectively (in turn associated with moderate, heavy and very heavy sparticle spectra).

The distinctive NUHM-seesaw scenarios associated with light H^0 bosons and a relatively heavy SUSY spectra induce very interesting and unique predictions for the $\mu - e$ conversion rates. Specifically, we have shown that in the large $M_{\text{SUSY}} = M_0 = M_{1/2}$ region (e.g. above 700 GeV), there is a strong enhancement in the Higgs-dominated rates, leading to a remarkable loss of correlation between the CRs in nuclei and the BRs of $\mu \rightarrow e\gamma$ decays. As we aimed at illustrating in Fig. 10, the departure from the linear correlation of these two observables can be sizable. It is worth stressing that if both these rates and θ_{13} are measured, values of $\text{BR}(\mu \rightarrow e\gamma)$ and $\text{CR}(\mu - e, \text{Ti})$ that clearly deviate from the expected SUSY-seesaw ratio in the photon-dominated case, can provide indirect information into the structure of the Higgs sector.

It is also important to remark that with the expected future sensitivities, $\mu - e$ conversion in nuclei maybe sensitive to LFV signals that lie beyond the reach of the future sensitivities to $\mu \rightarrow e\gamma$ decays. For example, this can occur for a heavy SUSY spectrum, and very small values of θ_{13} .

Finally, we considered the predictions for the ratio $\text{CR}(\mu - e, \text{Ti})/\text{BR}(\mu \rightarrow e\gamma)$ as a function of m_{H^0} in NUHM-seesaw scenarios, comparing the results with those obtained for the CMSSM-seesaw case. The most important conclusion to be drawn from this study (which is presented in Fig. 11) is that in the NUHM-seesaw one can observe a clear deviation from the constant prediction of the CMSSM-seesaw by as much as a factor close to 10. If such deviation is indeed observed, we can obtain some indirect hints regarding the SUSY Higgs sector.

In summary, with the expected future sensitivities, $\mu - e$ conversion in nuclei can clearly be more competitive for the study of LFV in SUSY-seesaw than $\mu \rightarrow e\gamma$, and certainly provide an important tool for the study of the Higgs sector.

Acknowledgements

We acknowledge S. Antusch for his participation in the initial stages of this work. We are grateful to S. Ritt for providing important information on the experimental status of

present bounds and future sensitivities of LFV muon decays and $\mu - e$ conversion rates in nuclei. We are also indebted to D.G. Cerd  o for valuable discussions on the NUHM scenarios. E. Arganda acknowledges the Spanish MEC for financial support under the grant AP2003-3776. The work of A. M. Teixeira has been supported by the French ANR project PHYS@COL&COS. This work was partially supported by the Spanish MEC under project FPA2006-05423 and by the regional ‘‘Comunidad de Madrid’’ HEPHACOS project.

A One-loop formulae for $\mu - e$ conversion in nuclei

In this appendix we collect all the analytical results of the SUSY one-loop diagrams that contribute to the $\mu - e$ conversion rates in nuclei. These are summarised by the photon-, Z -boson- and Higgs-boson- penguins and box diagrams in Figs. 12, 13, 14 and 15, respectively. In the following subsections we present the relevant formulae for each separate contribution. All the loop functions in the formulae are taken from [33, 41].

A.1 Form factors for the $\gamma\mu e$ vertex

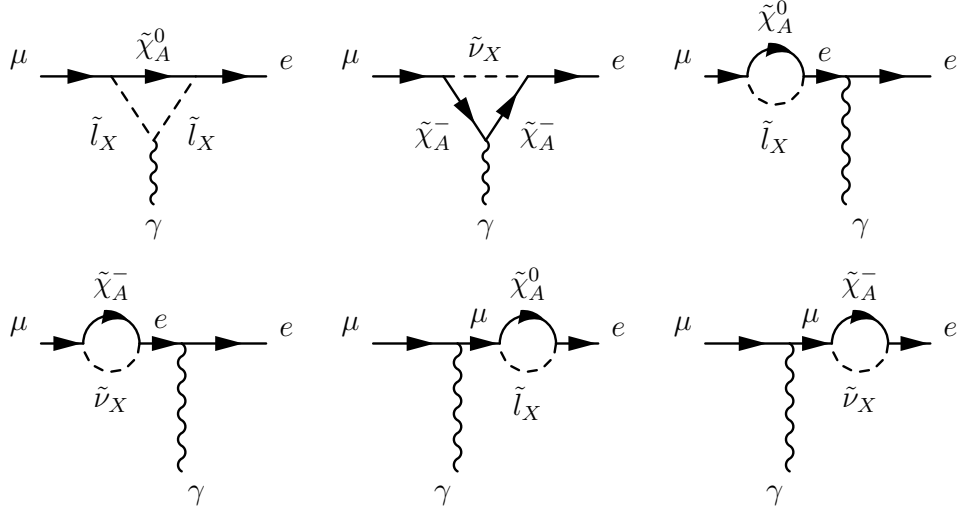


Figure 12: Relevant SUSY one-loop diagrams for the photon-mediated contributions to $\mu - e$ conversion in nuclei.

Our convention for the form factors $A_{1,2}^{L,R}$ defining the $\gamma\mu e$ vertex is as follows:

$$ie \left[q^2 \gamma_\alpha (A_1^L P_L + A_1^R P_R) + im_\mu \sigma_{\alpha\beta} q^\beta (A_a^L P_L + A_2^R P_R) \right], \quad (35)$$

where q is the off-shell photon momentum, $P_{L,R} = (1 \mp \gamma_5)/2$, e is the electromagnetic charge and m_μ is the muon mass.

In the SUSY-seesaw context there are one-loop contributions to these form factors that come from the chargino and neutralino sectors respectively,

$$A_a^{L,R} = A_a^{(n)L,R} + A_a^{(c)L,R}, \quad a = 1, 2. \quad (36)$$

The neutralino contributions are given by,

$$A_1^{(n)L} = \frac{1}{576\pi^2} N_{eAX}^R N_{\mu AX}^{R*} \frac{1}{m_{\tilde{l}_X}^2} \frac{2 - 9x_{AX} + 18x_{AX}^2 - 11x_{AX}^3 + 6x_{AX}^3 \log x_{AX}}{(1 - x_{AX})^4} \quad (37)$$

$$\begin{aligned} A_2^{(n)L} &= \frac{1}{32\pi^2} \frac{1}{m_{\tilde{l}_X}^2} \left[N_{eAX}^L N_{\mu AX}^{L*} \frac{1 - 6x_{AX} + 3x_{AX}^2 + 2x_{AX}^3 - 6x_{AX}^2 \log x_{AX}}{6(1 - x_{AX})^4} \right. \\ &+ N_{eAX}^R N_{\mu AX}^{R*} \frac{m_e}{m_\mu} \frac{1 - 6x_{AX} + 3x_{AX}^2 + 2x_{AX}^3 - 6x_{AX}^2 \log x_{AX}}{6(1 - x_{AX})^4} \\ &+ \left. N_{eAX}^L N_{\mu AX}^{R*} \frac{m_{\tilde{\chi}_A^0}}{m_\mu} \frac{1 - x_{AX}^2 + 2x_{AX} \log x_{AX}}{(1 - x_{AX})^3} \right], \end{aligned} \quad (38)$$

$$A_a^{(n)R} = A_a^{(n)L} \Big|_{L \leftrightarrow R}, \quad (39)$$

where $x_{AX} = m_{\tilde{\chi}_A^0}^2 / m_{\tilde{l}_X}^2$ and the indices are $A = 1, \dots, 4$, $X = 1, \dots, 6$.

The chargino contributions are given by

$$A_1^{(c)L} = -\frac{1}{576\pi^2} C_{eAX}^R C_{\mu AX}^{R*} \frac{1}{m_{\tilde{\nu}_X}^2} \frac{16 - 45x_{AX} + 36x_{AX}^2 - 7x_{AX}^3 + 6(2 - 3x_{AX}) \log x_{AX}}{(1 - x_{AX})^4}, \quad (40)$$

$$\begin{aligned} A_2^{(c)L} &= -\frac{1}{32\pi^2} \frac{1}{m_{\tilde{\nu}_X}^2} \left[C_{eAX}^L C_{\mu AX}^{L*} \frac{2 + 3x_{AX} - 6x_{AX}^2 + x_{AX}^3 + 6x_{AX} \log x_{AX}}{6(1 - x_{AX})^4} \right. \\ &+ C_{eAX}^R C_{\mu AX}^{R*} \frac{m_e}{m_\mu} \frac{2 + 3x_{AX} - 6x_{AX}^2 + x_{AX}^3 + 6x_{AX} \log x_{AX}}{6(1 - x_{AX})^4} \\ &+ \left. C_{eAX}^L C_{\mu AX}^{R*} \frac{m_{\tilde{\chi}_A^-}}{m_\mu} \frac{-3 + 4x_{AX} - x_{AX}^2 - 2 \log x_{AX}}{(1 - x_{AX})^3} \right], \end{aligned} \quad (41)$$

$$A_a^{(c)R} = A_a^{(c)L} \Big|_{L \leftrightarrow R}, \quad (42)$$

where in this case $x_{AX} = m_{\tilde{\chi}_A^-}^2 / m_{\tilde{\nu}_X}^2$ and the indices are $A = 1, 2$, $X = 1, 2, 3$. Notice that in both neutralino and chargino contributions a summation over the indices A and X is understood.

A.2 Form factors for the $Z\mu e$ vertex

Our convention for the form factors $F_{L,R}$ defining the $Z\mu e$ vertex is as follows:

$$-i\gamma_\mu [F_L P_L + F_R P_R]. \quad (43)$$

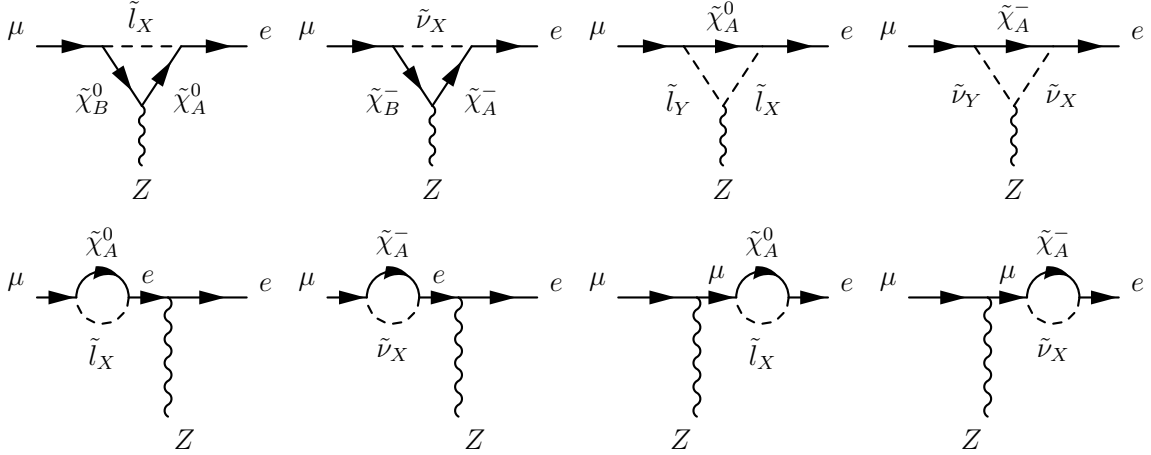


Figure 13: Relevant SUSY one-loop diagrams for the Z -mediated contributions to $\mu - e$ conversion in nuclei

The Z -boson form factors have also the two kinds of contributions, from neutralinos (n) and charginos (c),

$$F_{L(R)} = F_{L(R)}^{(n)} + F_{L(R)}^{(c)}. \quad (44)$$

The results for the corresponding form factors are the following:

$$F_L^{(n)} = -\frac{1}{16\pi^2} \left\{ N_{eBX}^R N_{\mu AX}^{R*} \left[2E_{BA}^{R(n)} C_{24}(m_{\tilde{l}_X}^2, m_{\tilde{\chi}_A^0}^2, m_{\tilde{\chi}_B^0}^2) - E_{BA}^{L(n)} m_{\tilde{\chi}_A^0} m_{\tilde{\chi}_B^0} C_0(m_{\tilde{l}_X}^2, m_{\tilde{\chi}_A^0}^2, m_{\tilde{\chi}_B^0}^2) \right] \right. \\ \left. + N_{eAX}^R N_{\mu AY}^{R*} \left[2Q_{XY}^{\tilde{l}} C_{24}(m_{\tilde{\chi}_A^0}^2, m_{\tilde{l}_X}^2, m_{\tilde{l}_Y}^2) \right] + N_{eAX}^R N_{\mu AX}^{R*} \left[Z_L^{(l)} B_1(m_{\tilde{\chi}_A^0}^2, m_{\tilde{l}_X}^2) \right] \right\}, \quad (45)$$

$$F_R^{(n)} = F_L^{(n)} \Big|_{L \leftrightarrow R}, \quad (46)$$

$$F_L^{(c)} = -\frac{1}{16\pi^2} \left\{ C_{eBX}^R C_{\mu AX}^{R*} \left[2E_{BA}^{R(c)} C_{24}(m_{\tilde{\nu}_X}^2, m_{\tilde{\chi}_A^-}^2, m_{\tilde{\chi}_B^-}^2) - E_{BA}^{L(c)} m_{\tilde{\chi}_A^-} m_{\tilde{\chi}_B^-} C_0(m_{\tilde{\nu}_X}^2, m_{\tilde{\chi}_A^-}^2, m_{\tilde{\chi}_B^-}^2) \right] \right. \\ \left. + C_{eAX}^R C_{\mu AY}^{R*} \left[2Q_{XY}^{\tilde{\nu}} C_{24}(m_{\tilde{\chi}_A^-}^2, m_{\tilde{\nu}_X}^2, m_{\tilde{\nu}_Y}^2) \right] + C_{eAX}^R C_{\mu AX}^{R*} \left[Z_L^{(l)} B_1(m_{\tilde{\chi}_A^-}^2, m_{\tilde{\nu}_X}^2) \right] \right\}, \quad (47)$$

$$F_R^{(c)} = F_L^{(c)} \Big|_{L \leftrightarrow R}, \quad (48)$$

where again the indices are $A, B = 1, \dots, 4$, $X, Y = 1, \dots, 6$ in the contributions from the neutralino sector and $A, B = 1, 2$, $X, Y = 1, 2, 3$ in the contributions from the chargino sector, and a summation over the various indices is understood.

A.3 Form factors for the $H\mu e$ vertex

Our convention for the form factors $H_{L,R}$ defining the $H\mu e$ vertex is as follows:

$$i\gamma_\mu [H_L P_L + H_R P_R]. \quad (49)$$

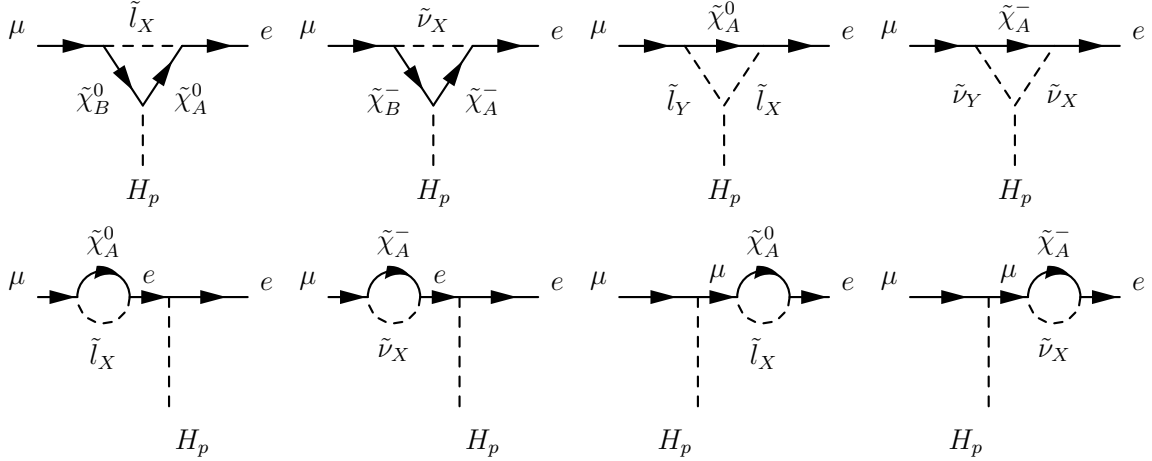


Figure 14: Relevant SUSY one-loop diagrams for the Higgs-mediated contributions to $\mu - e$ conversion in nuclei.

As in the previous cases, we separate the contributions from the neutralino and chargino sectors,

$$H_{L(R)} = H_{L(R),n}^{(p)} + H_{L(R),c}^{(p)}. \quad (50)$$

The results for the form factors are the following,

$$\begin{aligned}
H_{L,n}^{(p)} = & -\frac{1}{16\pi^2} \left\{ \left[B_0(m_{\tilde{\chi}_A^0}^2, m_{\tilde{\chi}_B^0}^2) + m_{\tilde{l}_X}^2 C_0(m_{\tilde{l}_X}^2, m_{\tilde{\chi}_A^0}^2, m_{\tilde{\chi}_B^0}^2) + m_\mu^2 C_{12}(m_{\tilde{l}_X}^2, m_{\tilde{\chi}_A^0}^2, m_{\tilde{\chi}_B^0}^2) \right. \right. \\
& + m_e^2 (C_{11} - C_{12})(m_{\tilde{l}_X}^2, m_{\tilde{\chi}_A^0}^2, m_{\tilde{\chi}_B^0}^2) \left. \right] N_{eAX}^L D_{R,AB}^{(p)} N_{\mu BX}^{R*} \\
& + m_e m_\mu (C_{11} + C_0)(m_{\tilde{l}_X}^2, m_{\tilde{\chi}_A^0}^2, m_{\tilde{\chi}_B^0}^2) N_{eAX}^R D_{L,AB}^{(p)} N_{\mu BX}^{L*} \\
& + m_e m_{\tilde{\chi}_B^0} (C_{11} - C_{12} + C_0)(m_{\tilde{l}_X}^2, m_{\tilde{\chi}_A^0}^2, m_{\tilde{\chi}_B^0}^2) N_{eAX}^R D_{L,AB}^{(p)} N_{\mu BX}^{R*} \\
& + m_\mu m_{\tilde{\chi}_B^0} C_{12}(m_{\tilde{l}_X}^2, m_{\tilde{\chi}_A^0}^2, m_{\tilde{\chi}_B^0}^2) N_{eAX}^L D_{R,AB}^{(p)} N_{\mu BX}^{L*} \\
& + m_e m_{\tilde{\chi}_A^0} (C_{11} - C_{12})(m_{\tilde{l}_X}^2, m_{\tilde{\chi}_A^0}^2, m_{\tilde{\chi}_B^0}^2) N_{eAX}^R D_{R,AB}^{(p)} N_{\mu BX}^{R*} \\
& + m_\mu m_{\tilde{\chi}_A^0} (C_{12} + C_0)(m_{\tilde{l}_X}^2, m_{\tilde{\chi}_A^0}^2, m_{\tilde{\chi}_B^0}^2) N_{eAX}^L D_{L,AB}^{(p)} N_{\mu BX}^{L*} \\
& + m_{\tilde{\chi}_A^0} m_{\tilde{\chi}_B^0} C_0(m_{\tilde{l}_X}^2, m_{\tilde{\chi}_A^0}^2, m_{\tilde{\chi}_B^0}^2) N_{eAX}^L D_{L,AB}^{(p)} N_{\mu BX}^{R*} \\
& + G_{XY}^{(p)\tilde{l}} \left[-m_e (C_{11} - C_{12})(m_{\tilde{\chi}_A^0}^2, m_{\tilde{l}_X}^2, m_{\tilde{l}_Y}^2) N_{eAX}^R N_{\mu AY}^{R*} \right. \\
& - m_\mu C_{12}(m_{\tilde{\chi}_A^0}^2, m_{\tilde{l}_X}^2, m_{\tilde{l}_Y}^2) N_{eAX}^L N_{\mu AY}^{L*} + m_{\tilde{\chi}_A^0} C_0(m_{\tilde{\chi}_A^0}^2, m_{\tilde{l}_X}^2, m_{\tilde{l}_Y}^2) N_{eAX}^L N_{\mu AY}^{R*} \left. \right] \\
& + \frac{S_{L,j}^{(p)}}{m_e^2 - m_\mu^2} \left[-m_e^2 B_1(m_{\tilde{\chi}_A^0}^2, m_{\tilde{l}_X}^2) N_{eAX}^L N_{\mu AX}^{L*} + m_e m_{\tilde{\chi}_A^0} B_0(m_{\tilde{\chi}_A^0}^2, m_{\tilde{l}_X}^2) N_{eAX}^R N_{\mu AX}^{L*} \right. \\
& - m_e m_\mu B_1(m_{\tilde{\chi}_A^0}^2, m_{\tilde{l}_X}^2) N_{eAX}^R N_{\mu AX}^{R*} + m_\mu m_{\tilde{\chi}_A^0} B_0(m_{\tilde{\chi}_A^0}^2, m_{\tilde{l}_X}^2) N_{eAX}^L N_{\mu AX}^{R*} \left. \right] \\
& + \frac{S_{L,i}^{(p)}}{m_\mu^2 - m_e^2} \left[-m_\mu^2 B_1(m_{\tilde{\chi}_A^0}^2, m_{\tilde{l}_X}^2) N_{eAX}^R N_{\mu AX}^{R*} + m_\mu m_{\tilde{\chi}_A^0} B_0(m_{\tilde{\chi}_A^0}^2, m_{\tilde{l}_X}^2) N_{eAX}^R N_{\mu AX}^{L*} \right. \\
& - m_e m_\mu B_1(m_{\tilde{\chi}_A^0}^2, m_{\tilde{l}_X}^2) N_{eAX}^L N_{\mu AX}^{L*} + m_e m_{\tilde{\chi}_A^0} B_0(m_{\tilde{\chi}_A^0}^2, m_{\tilde{l}_X}^2) N_{eAX}^L N_{\mu AX}^{R*} \left. \right] \left. \right\}, \quad (51)
\end{aligned}$$

$$H_{R,n}^{(p)} = H_{L,n}^{(p)} \Big|_{L \leftrightarrow R} \quad p = 1, 2, 3. \quad (52)$$

Correspondingly, the result for the chargino contribution $H_{L(R),c}^{(p)}$ can be obtained from the previous $H_{L(R),n}^{(p)}$ by replacing everywhere,

$$\begin{aligned}
\tilde{l} & \rightarrow \tilde{\nu} \\
\tilde{\chi}^0 & \rightarrow \tilde{\chi}^- \\
N^{L(R)} & \rightarrow C^{L(R)} \\
D_{L(R)} & \rightarrow W_{L(R)}
\end{aligned}$$

In the previous formulae, the index p refers to the each of the Higgs bosons. Concretely, $H_p = h^0, H^0, A^0$ for $p = 1, 2, 3$, respectively. The other indices are again $A, B = 1, \dots, 4$, $X, Y = 1, \dots, 6$ in the contributions from the neutralino sector and $A, B = 1, 2$ and $X, Y = 1, 2, 3$ in the contributions from the chargino sector. A summation over all the indices is also understood.

A.4 Contributions from box diagrams

We follow here a similar notation as in the previous formulae for the separate contributions from the neutralino and the chargino sectors. Our convention for the box diagrams at the quark level is iB_q .

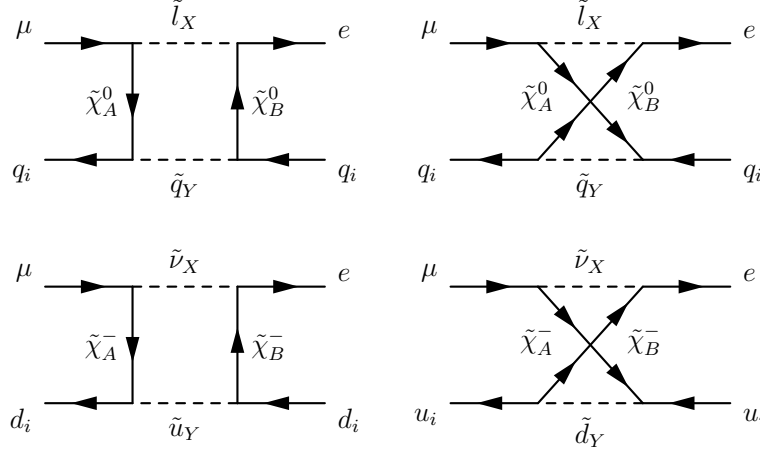


Figure 15: Box diagrams contributing to $\mu - e$ conversion in nuclei.

The results for the vector contributions are the following:

$$B_q^{(n)LV} = \frac{1}{16\pi^2} \left\{ -\frac{1}{8} \tilde{D}_0(m_{\tilde{\chi}_A^0}^2, m_{\tilde{\chi}_B^0}^2, m_{\tilde{l}_X}^2, m_{\tilde{q}_Y}^2) \times \left[N_{\mu AX}^{R(l)*} N_{e BX}^{R(l)} N_{q AY}^{R(q)*} N_{q BY}^{R(q)} \right. \right. \\ \left. \left. - N_{\mu AX}^{R(l)*} N_{e BX}^{R(l)} N_{q AY}^{L(q)} N_{q BY}^{L(q)*} \right] + \frac{1}{4} m_{\tilde{\chi}_A^0} m_{\tilde{\chi}_B^0} D_0(m_{\tilde{\chi}_A^0}^2, m_{\tilde{\chi}_B^0}^2, m_{\tilde{l}_X}^2, m_{\tilde{q}_Y}^2) \times \right. \\ \left. \left[N_{\mu AX}^{R(l)*} N_{e BX}^{R(l)} N_{q AY}^{L(q)} N_{q BY}^{L(q)*} - N_{\mu AX}^{R(l)*} N_{e BX}^{R(l)} N_{q AY}^{R(q)*} N_{q BY}^{R(q)} \right] \right\}, \quad (53)$$

$$B_q^{(n)RV} = B_q^{(n)LV} \Big|_{L \leftrightarrow R}, \quad (54)$$

$$B_d^{(c)LV} = \frac{1}{16\pi^2} \left\{ -\frac{1}{8} \tilde{D}_0(m_{\tilde{\chi}_A^-}^2, m_{\tilde{\chi}_B^-}^2, m_{\tilde{\nu}_X}^2, m_{\tilde{u}_Y}^2) C_{\mu AX}^{R(l)*} C_{e BX}^{R(l)} C_{d AY}^{R(d)} C_{d BY}^{R(d)*} \right. \\ \left. + \frac{1}{4} m_{\tilde{\chi}_A^-} m_{\tilde{\chi}_B^-} D_0(m_{\tilde{\chi}_A^-}^2, m_{\tilde{\chi}_B^-}^2, m_{\tilde{\nu}_X}^2, m_{\tilde{u}_Y}^2) C_{\mu AX}^{R(l)*} C_{e BX}^{R(l)} C_{d AY}^{L(d)} C_{d BY}^{L(d)*} \right\}, \quad (55)$$

$$B_u^{(c)LV} = \frac{1}{16\pi^2} \left\{ \frac{1}{8} \tilde{D}_0(m_{\tilde{\chi}_A^-}^2, m_{\tilde{\chi}_B^-}^2, m_{\tilde{\nu}_X}^2, m_{\tilde{d}_Y}^2) C_{\mu AX}^{R(l)*} C_{e BX}^{R(l)} C_{u AY}^{L(u)*} C_{u BY}^{L(u)} \right. \\ \left. + \frac{1}{4} m_{\tilde{\chi}_A^-} m_{\tilde{\chi}_B^-} D_0(m_{\tilde{\chi}_A^-}^2, m_{\tilde{\chi}_B^-}^2, m_{\tilde{\nu}_X}^2, m_{\tilde{d}_Y}^2) C_{\mu AX}^{R(l)*} C_{e BX}^{R(l)} C_{u AY}^{R(u)*} C_{u BY}^{R(u)} \right\}, \quad (56)$$

$$B_{u,d}^{(c)RV} = B_{u,d}^{(c)LV} \Big|_{L \leftrightarrow R}. \quad (57)$$

The results for the scalar contributions are given by:

$$\begin{aligned}
B_q^{(n)LS} &= \frac{1}{16\pi^2} \left\{ \frac{1}{4} \tilde{D}_0(m_{\tilde{\chi}_A^0}^2, m_{\tilde{\chi}_B^0}^2, m_{\tilde{l}_X}^2, m_{\tilde{q}_Y}^2) \times \left[N_{\mu AX}^{R(l)*} N_{e BX}^{L(l)} N_{q AY}^{R(q)} N_{q BY}^{L(q)*} \right. \right. \\
&\quad \left. \left. + N_{\mu AX}^{R(l)*} N_{e BX}^{L(l)} N_{q AY}^{L(q)*} N_{q BY}^{R(q)} \right] + \frac{1}{4} m_{\tilde{\chi}_A^0} m_{\tilde{\chi}_B^0} D_0(m_{\tilde{\chi}_A^0}^2, m_{\tilde{\chi}_B^0}^2, m_{\tilde{l}_X}^2, m_{\tilde{q}_Y}^2) \times \right. \\
&\quad \left. \left[N_{\mu AX}^{R(l)*} N_{e BX}^{L(l)} N_{q AY}^{L(q)} N_{q BY}^{R(q)*} + N_{\mu AX}^{R(l)*} N_{e BX}^{L(l)} N_{q AY}^{R(q)*} N_{q BY}^{L(q)} \right] \right\}, \tag{58}
\end{aligned}$$

$$B_q^{(n)RS} = B_q^{(n)LS} \Big|_{L \leftrightarrow R}, \tag{59}$$

$$\begin{aligned}
B_d^{(c)LS} &= \frac{1}{16\pi^2} \left\{ \frac{1}{4} \tilde{D}_0(m_{\tilde{\chi}_A^-}^2, m_{\tilde{\chi}_B^-}^2, m_{\tilde{\nu}_X}^2, m_{\tilde{u}_Y}^2) C_{\mu AX}^{R(l)*} C_{e BX}^{L(l)} C_{d AY}^{R(d)} C_{d BY}^{L(d)*} \right. \\
&\quad \left. + \frac{1}{4} m_{\tilde{\chi}_A^-} m_{\tilde{\chi}_B^-} D_0(m_{\tilde{\chi}_A^-}^2, m_{\tilde{\chi}_B^-}^2, m_{\tilde{\nu}_X}^2, m_{\tilde{u}_Y}^2) C_{\mu AX}^{R(l)*} C_{e BX}^{L(l)} C_{d AY}^{L(d)} C_{d BY}^{R(d)*} \right\}, \tag{60}
\end{aligned}$$

$$\begin{aligned}
B_u^{(c)LS} &= \frac{1}{16\pi^2} \left\{ \frac{1}{4} \tilde{D}_0(m_{\tilde{\chi}_A^-}^2, m_{\tilde{\chi}_B^-}^2, m_{\tilde{\nu}_X}^2, m_{\tilde{d}_Y}^2) C_{\mu AX}^{R(l)*} C_{e BX}^{L(l)} C_{u AY}^{L(u)*} C_{u BY}^{R(u)} \right. \\
&\quad \left. + \frac{1}{4} m_{\tilde{\chi}_A^-} m_{\tilde{\chi}_B^-} D_0(m_{\tilde{\chi}_A^-}^2, m_{\tilde{\chi}_B^-}^2, m_{\tilde{\nu}_X}^2, m_{\tilde{d}_Y}^2) C_{\mu AX}^{R(l)*} C_{e BX}^{L(l)} C_{u AY}^{R(u)*} C_{u BY}^{L(u)} \right\}, \tag{61}
\end{aligned}$$

$$B_{u,d}^{(c)RS} = B_{u,d}^{(c)LS} \Big|_{L \leftrightarrow R}. \tag{62}$$

The indices in the previous formulae are again, $A, B = 1, \dots, 4$, $X, Y = 1, \dots, 6$ in the contributions from the neutralino sector and $A, B = 1, 2$, $X, Y = 1, 2, 3$ in the contributions from the chargino sector. A summation over all the indices is also understood.

B Relevant couplings for $\mu - e$ conversion in nuclei

In this appendix we collect the formulae for the couplings that are relevant in this work. We follow the same notation for the couplings as in [33] and include here some of the formulae presented there, for completeness. The couplings are expressed in the physical eigenstate basis, for all the MSSM sectors involved: sleptons \tilde{l}_X ($X = 1, \dots, 6$), sneutrinos $\tilde{\nu}_X$ ($X = 1, 2, 3$), neutralinos $\tilde{\chi}_A^0$ ($A = 1, \dots, 4$), charginos $\tilde{\chi}_A^\pm$ ($A = 1, 2$) and the neutral Higgs bosons H_p ($p = 1, 2, 3$) $= h^0, H^0, A^0$. Notice that the case $H_p = A^0$ is given for completeness but, as explained in the text, it does not contribute to the $\mu - e$ conversion in nuclei in the coherent approximation assumed in the present work.

The notation for the SM parameters that appear in the following couplings is as follows: g is the $SU(2)$ gauge coupling, m_f is the fermion mass, m_W , m_Z are the W -boson and Z -boson masses, respectively, and θ_W is the weak angle.

B.1 Neutralino couplings

The couplings for neutralinos that enter in the one-loop diagrams computed here are the following:

$$N_{iAX}^{L(l)} = -g\sqrt{2} \left\{ \frac{m_{l_i}}{2m_W \cos \beta} N_{A3}^* R_{(1,3,5)X}^{(l)} + \tan \theta_W N_{A1}^* R_{(2,4,6)X}^{(l)} \right\}, \quad (63)$$

$$N_{iAX}^{R(l)} = -g\sqrt{2} \left\{ -\frac{1}{2} (\tan \theta_W N_{A1} + N_{A2}) R_{(1,3,5)X}^{(l)} + \frac{m_{l_i}}{2m_W \cos \beta} N_{A3} R_{(2,4,6)X}^{(l)} \right\}, \quad (64)$$

$$N_{iAX}^{L(d)} = -g\sqrt{2} \left\{ \frac{m_{d_i}}{2m_W \cos \beta} N_{A3}^* R_{(1,3,5)X}^{(d)} + \frac{1}{3} \tan \theta_W N_{A1}^* R_{(2,4,6)X}^{(d)} \right\}, \quad (65)$$

$$N_{iAX}^{R(d)} = -g\sqrt{2} \left\{ -\frac{1}{2} \left(-\frac{1}{3} \tan \theta_W N_{A1} + N_{A2} \right) R_{(1,3,5)X}^{(d)} + \frac{m_{d_i}}{2m_W \cos \beta} N_{A3} R_{(2,4,6)X}^{(d)} \right\} \quad (66)$$

$$N_{iAX}^{L(u)} = -g\sqrt{2} \left\{ \frac{m_{u_i}}{2m_W \sin \beta} N_{A4}^* R_{(1,3,5)X}^{(u)} - \frac{2}{3} \tan \theta_W N_{A1}^* R_{(2,4,6)X}^{(u)} \right\}, \quad (67)$$

$$N_{iAX}^{R(u)} = -g\sqrt{2} \left\{ -\frac{1}{2} \left(\frac{2}{3} \tan \theta_W N_{A1} - N_{A2} \right) R_{(1,3,5)X}^{(u)} + \frac{m_{u_i}}{2m_W \sin \beta} N_{A4} R_{(2,4,6)X}^{(u)} \right\}. \quad (68)$$

Here, $R^{(l)}$, $R^{(d)}$, $R^{(u)}$ are the 6×6 rotation matrices for the charged slepton, down squark and up squark sectors, respectively, and N is the 4×4 rotation matrix for the neutralino sector. For completeness, we have written the full set of couplings, including the three fermion generations. The displayed notation for the sfermion rotation matrices with three entries $R_{(, ,)}$ correspond with the three generic possibilities to fermion index i . The fermion masses are correspondingly, $m_{l_i} = m_e, m_\mu, m_\tau$; $m_{d_i} = m_d, m_s, m_b$ and $m_{u_i} = m_u, m_c, m_t$. Notice also that, although we use the same notation for the squark and slepton sectors, and since we have not included mixing in the quark sector, the 6×6 rotation matrices $R^{(d)}$ and $R^{(u)}$ are block diagonal in flavour space and only $L - R$ mixing occurs in that case.

B.2 Chargino couplings

The couplings for charginos that are present in the one-loop diagrams computed here are the following:

$$C_{iAX}^{L(l)} = g \frac{m_{l_i}}{\sqrt{2}m_W \cos \beta} U_{A2}^* R_{(1,2,3)X}^{(\nu)}, \quad (69)$$

$$C_{iAX}^{R(l)} = -g V_{A1} R_{(1,2,3)X}^{(\nu)}, \quad (70)$$

$$C_{iAX}^{L(d)} = g \frac{m_{d_i}}{\sqrt{2}m_W \cos \beta} U_{A2}^* R_{(1,3,5)X}^{(u)}, \quad (71)$$

$$C_{iAX}^{R(d)} = -g V_{A1} R_{(1,3,5)X}^{(u)} + g \frac{m_{u_i}}{\sqrt{2}m_W \sin \beta} V_{A2} R_{(2,4,6)X}^{(u)}, \quad (72)$$

$$C_{iAX}^{L(u)} = g \frac{m_{u_i}}{\sqrt{2}m_W \sin \beta} V_{A2}^* R_{(1,3,5)X}^{(d)}, \quad (73)$$

$$C_{iAX}^{R(u)} = -g U_{A1} R_{(1,3,5)X}^{(d)} + g \frac{m_{d_i}}{\sqrt{2}m_W \cos \beta} U_{A2} R_{(2,4,6)X}^{(d)}. \quad (74)$$

Here $R^{(\nu)}$ is the 3×3 rotation matrix for the sneutrino sector, and U and V are the 2×2 rotation matrices in the chargino sector. The displayed notation for the three entries in the sfermion rotation matrices is as in the previous neutralino couplings. The rotation matrices for neutralinos and charginos can be found in [42] and [43].

B.3 Z boson couplings

$Z\tilde{\chi}_A^0\tilde{\chi}_B^0$ coupling:

$$E_{AB}^{L(n)} = \frac{g}{\cos \theta_W} O_{AB}^{\prime L} = \frac{g}{c_W} \left(-\frac{1}{2} N_{A3} N_{B3}^* + \frac{1}{2} N_{A4} N_{B4}^* \right), \quad (75)$$

$$E_{AB}^{R(n)} = \frac{g}{\cos \theta_W} O_{AB}^{\prime R} = -\frac{g}{c_W} \left(-\frac{1}{2} N_{A3}^* N_{B3} + \frac{1}{2} N_{A4}^* N_{B4} \right). \quad (76)$$

$Z\tilde{\chi}_A^+\tilde{\chi}_B^-$ coupling:

$$E_{AB}^{L(c)} = -\frac{g}{\cos \theta_W} O_{AB}^{\prime R} = -\frac{g}{c_W} \left[-\left(\frac{1}{2} - s_W^2 \right) U_{A2}^* U_{B2} - c_W^2 U_{A1}^* U_{B1} \right], \quad (77)$$

$$E_{AB}^{R(c)} = -\frac{g}{\cos \theta_W} O_{AB}^{\prime L} = -\frac{g}{c_W} \left[-\left(\frac{1}{2} - s_W^2 \right) V_{A2} V_{B2}^* - c_W^2 V_{A1} V_{B1}^* \right]. \quad (78)$$

$Z\tilde{l}_X\tilde{l}_Y$ coupling:

$$Q_{XY}^{(\tilde{l})} = -\frac{g}{c_W} \sum_{k=1}^3 \left[\left(-\frac{1}{2} + s_W^2 \right) R_{2k-1,X}^{(l)*} R_{2k-1,Y}^{(l)} + s_W^2 R_{2k,X}^{(l)*} R_{2k,Y}^{(l)} \right]. \quad (79)$$

$Z\tilde{\nu}_X\tilde{\nu}_Y$ coupling:

$$Q_{XY}^{(\tilde{\nu})} = -\frac{g}{2c_W}\delta_{XY}. \quad (80)$$

$Z\bar{l}l$ coupling:

$$Z_L^{(l)} = -\frac{g}{c_W} \left[-\frac{1}{2} + s_W^2 \right], \quad (81)$$

$$Z_R^{(l)} = -\frac{g}{c_W} s_W^2. \quad (82)$$

$Z\bar{q}q$ coupling:

$$Z_L^{(q)} = -\frac{g}{c_W} [T_3^q - Q_q s_W^2], \quad (83)$$

$$Z_R^{(q)} = \frac{g}{c_W} Q_q s_W^2. \quad (84)$$

We have used here the short notation $s_W = \sin \theta_W$ and $c_W = \cos \theta_W$.

B.4 Higgs boson couplings

$H_p\tilde{\chi}_A^0\tilde{\chi}_B^0$ coupling:

$$\begin{aligned} D_{L,AB}^{(p)} &= -\frac{g}{2\cos\theta_W} \left[(s_W N_{B1}^* - c_W N_{B2}^*) \left(\sigma_1^{(p)} N_{A3}^* + \sigma_2^{(p)} N_{A4}^* \right) \right. \\ &\quad \left. + (s_W N_{A1}^* - c_W N_{A2}^*) \left(\sigma_1^{(p)} N_{B3}^* + \sigma_2^{(p)} N_{B4}^* \right) \right], \end{aligned} \quad (85)$$

$$D_{R,AB}^{(p)} = D_{L,AB}^{(p)*}. \quad (86)$$

$H_p\tilde{\chi}_A^+\tilde{\chi}_B^-$ coupling:

$$W_{L,AB}^{(p)} = -\frac{g}{\sqrt{2}} \left[-\sigma_1^{(p)} U_{B2}^* V_{A1}^* + \sigma_2^{(p)} U_{B1}^* V_{A2}^* \right], \quad (87)$$

$$W_{R,AB}^{(p)} = -\frac{g}{\sqrt{2}} \left[-\sigma_1^{(p)*} U_{A2} V_{B1} + \sigma_2^{(p)*} U_{A1} V_{B2} \right]. \quad (88)$$

$H_p\tilde{l}_X\tilde{l}_Y$ coupling:

$$\begin{aligned} G_{XY}^{p(\tilde{l})} &= -g \left[g_{LL,e}^{(p)} R_{1X}^{*(l)} R_{1Y}^{(l)} + g_{RR,e}^{(p)} R_{2X}^{*(l)} R_{2Y}^{(l)} + g_{LR,e}^{(p)} R_{1X}^{*(l)} R_{2Y}^{(l)} + g_{RL,e}^{(p)} R_{2X}^{*(l)} R_{1Y}^{(l)} \right. \\ &\quad + g_{LL,\mu}^{(p)} R_{3X}^{*(l)} R_{3Y}^{(l)} + g_{RR,\mu}^{(p)} R_{4X}^{*(l)} R_{4Y}^{(l)} + g_{LR,\mu}^{(p)} R_{3X}^{*(l)} R_{4Y}^{(l)} + g_{RL,\mu}^{(p)} R_{4X}^{*(l)} R_{3Y}^{(l)} \\ &\quad \left. + g_{LL,\tau}^{(p)} R_{5X}^{*(l)} R_{5Y}^{(l)} + g_{RR,\tau}^{(p)} R_{6X}^{*(l)} R_{6Y}^{(l)} + g_{LR,\tau}^{(p)} R_{5X}^{*(l)} R_{6Y}^{(l)} + g_{RL,\tau}^{(p)} R_{6X}^{*(l)} R_{5Y}^{(l)} \right], \end{aligned} \quad (89)$$

with

$$g_{LL,l}^{(p)} = \frac{m_Z}{\cos \theta_W} \sigma_3^{(p)} \left(\frac{1}{2} - \sin^2 \theta_W \right) + \frac{m_l^2}{m_W \cos \beta} \sigma_4^{(p)}, \quad (90)$$

$$g_{RR,l}^{(p)} = \frac{m_Z}{\cos \theta_W} \sigma_3^{(p)} (\sin^2 \theta_W) + \frac{m_l^2}{m_W \cos \beta} \sigma_4^{(p)}, \quad (91)$$

$$g_{LR,l}^{(p)} = \left(-\sigma_1^{(p)} A_l - \sigma_2^{(p)*} \mu \right) \frac{m_l}{2m_W \cos \beta}, \quad (92)$$

$$g_{RL,l}^{(p)} = g_{LR,l}^{(p)*}, \quad (93)$$

with $A_l = (A_l)^{ii}/(Y_l)^{ii}$ (at the EW scale), $i = 1, 2, 3$ for $l = e, \mu, \tau$, respectively.

$H_p \tilde{\nu}_X \tilde{\nu}_Y$ coupling:

$$G_{XY}^{p(\tilde{\nu})} = -g \left[g_{LL,\nu}^{(p)} R_{1X}^{*(\nu)} R_{1Y}^{(\nu)} + g_{LL,\nu}^{(p)} R_{2X}^{*(\nu)} R_{2Y}^{(\nu)} + g_{LL,\nu}^{(p)} R_{3X}^{*(\nu)} R_{3Y}^{(\nu)} \right], \quad (94)$$

with

$$g_{LL,\nu}^{(p)} = -\frac{m_Z}{2 \cos \theta_W} \sigma_3^{(p)}. \quad (95)$$

$H_p \bar{l} l$ coupling:

$$S_{L,l}^{(p)} = g \frac{m_{l_i}}{2m_W \cos \beta} \sigma_1^{(p)*}, \quad (96)$$

$$S_{R,l}^{(p)} = S_{L,l}^{(p)*}. \quad (97)$$

$H_p \bar{d} d$ coupling:

$$S_{L,d}^{(p)} = g \frac{m_{d_i}}{2m_W \cos \beta} \sigma_1^{(p)*}, \quad (98)$$

$$S_{R,d}^{(p)} = S_{L,d}^{(p)*}. \quad (99)$$

$H_p \bar{u} u$ coupling:

$$S_{L,u}^{(p)} = -g \frac{m_{u_i}}{2m_W \sin \beta} \sigma_2^{(p)*}, \quad (100)$$

$$S_{R,u}^{(p)} = S_{L,u}^{(p)*}. \quad (101)$$

In all the above equations,

$$\sigma_1^{(p)} = \begin{pmatrix} \sin \alpha \\ -\cos \alpha \\ i \sin \beta \end{pmatrix}, \quad (102)$$

$$\sigma_2^{(p)} = \begin{pmatrix} \cos \alpha \\ \sin \alpha \\ -i \cos \beta \end{pmatrix}, \quad (103)$$

$$\sigma_3^{(p)} = \begin{pmatrix} \sin(\alpha + \beta) \\ -\cos(\alpha + \beta) \\ 0 \end{pmatrix}, \quad (104)$$

$$\sigma_4^{(p)} = \begin{pmatrix} -\sin \alpha \\ \cos \alpha \\ 0 \end{pmatrix}, \quad (105)$$

$$\sigma_5^{(p)} = \begin{pmatrix} -\cos(\beta - \alpha) \\ \sin(\beta - \alpha) \\ i \cos 2\beta \end{pmatrix}. \quad (106)$$

We have also used here the standard notation for the low-energy MSSM soft-gaugino-mass parameters $M_{1,2}$ and the μ parameter.

References

- [1] B. T. Cleveland *et al.*, *Astrophys. J.* **496** (1998) 505; W. Hampel *et al.*, *Phys. Lett. B* **447** (1999) 127; Q. R. Ahmad *et al.* [SNO Collaboration], *Phys. Rev. Lett.* **87** (2001) 071301 [arXiv:nucl-ex/0106015]; Q. R. Ahmad *et al.* [SNO Collaboration], *Phys. Rev. Lett.* **89** (2002) 011302 [arXiv:nucl-ex/0204009]; R. Becker-Szendy *et al.*, *Nucl. Phys. Proc. Suppl.* **38** (1995) 331; Y. Fukuda *et al.* [Kamiokande Collaboration], *Phys. Lett. B* **335** (1994) 237; Y. Ashie *et al.* [Super-Kamiokande Collaboration], *Phys. Rev. Lett.* **93** (2004) 101801 [arXiv:hep-ex/0404034]; T. Araki *et al.* [KamLAND Collaboration], *Phys. Rev. Lett.* **94** (2005) 081801 [arXiv:hep-ex/0406035]; E. Aliu *et al.* [K2K Collaboration], *Phys. Rev. Lett.* **94** (2005) 081802 [arXiv:hep-ex/0411038]; T. Araki *et al.* [KamLAND Collaboration], *Phys. Rev. Lett.* **94** (2005) 081801 [arXiv:hep-ex/0406035].
- [2] W. M. Yao *et al.* [Particle Data Group], *J. Phys. G* **33** (2006) 1.
- [3] Y. Kuno and Y. Okada, *Rev. Mod. Phys.* **73** (2001) 151 [arXiv:hep-ph/9909265].

- [4] P. Minkowski, Phys. Lett. B **67** (1977) 421; M. Gell-Mann, P. Ramond and R. Slansky, in *Complex Spinors and Unified Theories* eds. P. Van. Nieuwenhuizen and D. Z. Freedman, *Supergravity* (North-Holland, Amsterdam, 1979), p.315 [Print-80-0576 (CERN)]; T. Yanagida, in *Proceedings of the Workshop on the Unified Theory and the Baryon Numebr in the Universe*, eds. O. Sawada and A. Sugamoto (KEK, Tsukuba, 1979), p.95; S. L. Glashow, in *Quarks and Leptons*, eds. M. Lévy et al. (Plenum Press, New York, 1980), p.687; R. N. Mohapatra and G. Senjanović, Phys. Rev. Lett. **44** (1980) 912.
- [5] R. Barbieri, D. V. Nanopolous, G. Morchio and F. Strocchi, Phys. Lett. B **90** (1980) 91; R. E. Marshak and R. N. Mohapatra, *Invited talk given at Orbis Scientiae, Coral Gables, Fla., Jan. 14-17, 1980*, VPI-HEP-80/02; T. P. Cheng and L. F. Li, Phys. Rev. D **22** (1980) 2860; M. Magg and C. Wetterich, Phys. Lett. B **94** (1980) 61; G. Lazarides, Q. Shafi and C. Wetterich, Nucl. Phys. B **181** (1981) 287; J. Schechter and J. W. F. Valle, Phys. Rev. D **22** (1980) 2227; R. N. Mohapatra and G. Senjanovic, Phys. Rev. D **23** (1981) 165. E. Ma and U. Sarkar, Phys. Rev. Lett. **80** (1998) 5716 [arXiv:hep-ph/9802445].
- [6] F. Borzumati and A. Masiero, Phys. Rev. Lett. **57** (1986) 961.
- [7] M. L. Brooks *et al.* [MEGA Collaboration], Phys. Rev. Lett. **83** (1999) 1521 [arXiv:hep-ex/9905013].
- [8] U. Bellgardt *et al.* [SINDRUM Collaboration], Nucl. Phys. B **299** (1988) 1.
- [9] C. Dohmen *et al.* [SINDRUM II Collaboration.], Phys. Lett. B **317** (1993) 631.
- [10] W. Bertl *et al.*, Eur. Phys. J. C **47** (2006) 337.
- [11] S. Ritt [MEG Collaboration], Nucl. Phys. Proc. Suppl. **162** (2006) 279.
- [12] S. Ritt, *private communication*.
- [13] The PRIME working group, “Search for the $\mu - e$ Conversion Process at an Ultimate Sensitivity of the Order of 10^{18} with PRISM”, unpublished; LOI to J-PARC 50-GeV PS, LOI-25, <http://psux1.kek.jp/jhf-np/LOIlist/LOIlist.html>
- [14] G. L. Kane, C. F. Kolda, L. Roszkowski and J. D. Wells, Phys. Rev. D **49** (1994) 6173 [arXiv:hep-ph/9312272].

- [15] J. R. Ellis, K. A. Olive and Y. Santoso, Phys. Lett. B **539** (2002) 107 [arXiv:hep-ph/0204192]; J. R. Ellis, T. Falk, K. A. Olive and Y. Santoso, Nucl. Phys. B **652** (2003) 259 [arXiv:hep-ph/0210205]; M. Olechowski and S. Pokorski, Phys. Lett. B **344** (1995) 201 [arXiv:hep-ph/9407404]; V. Berezhinsky, A. Bottino, J. R. Ellis, N. Fornengo, G. Mignola and S. Scopel, Astropart. Phys. **5** (1996) 1 [arXiv:hep-ph/9508249]; M. Drees, M. M. Nojiri, D. P. Roy and Y. Yamada, Phys. Rev. D **56** (1997) 276 [Erratum-ibid. D **64** (2001) 039901] [arXiv:hep-ph/9701219]; M. Drees, Y. G. Kim, M. M. Nojiri, D. Toya, K. Hasuko and T. Kobayashi, Phys. Rev. D **63** (2001) 035008 [arXiv:hep-ph/0007202]; P. Nath and R. Arnowitt, Phys. Rev. D **56** (1997) 2820 [arXiv:hep-ph/9701301]; J. R. Ellis, T. Falk, G. Ganis, K. A. Olive and M. Schmitt, Phys. Rev. D **58** (1998) 095002 [arXiv:hep-ph/9801445]; J. R. Ellis, T. Falk, G. Ganis and K. A. Olive, Phys. Rev. D **62** (2000) 075010 [arXiv:hep-ph/0004169]; A. Bottino, F. Donato, N. Fornengo and S. Scopel, Phys. Rev. D **63** (2001) 12500 [arXiv:hep-ph/0010203]; S. Profumo, Phys. Rev. D **68** (2003) 015006 [arXiv:hep-ph/0304071]; D. G. Cerdeno and C. Munoz, JHEP **0410** (2004) 015 [arXiv:hep-ph/0405057]; H. Baer, A. Mustafayev, S. Profumo, A. Belyaev and X. Tata, JHEP **0507** (2005) 065 [arXiv:hep-ph/0504001]; J. R. Ellis, S. Heinemeyer, K. A. Olive and G. Weiglein, arXiv:0706.0977 [hep-ph].
- [16] J. Hisano, T. Moroi, K. Tobe and M. Yamaguchi, Phys. Rev. D **53** (1996) 2442 [arXiv:hep-ph/9510309].
- [17] R. Kitano, M. Koike, S. Komine and Y. Okada, Phys. Lett. B **575** (2003) 300 [arXiv:hep-ph/0308021].
- [18] M. C. González-García and C. Peña-Garay, Phys. Rev. D **68** (2003) 093003 [arXiv:hep-ph/0306001]; M. Maltoni, T. Schwetz, M. A. Tortola and J. W. F. Valle, New J. Phys. **6** (2004) 122 [arXiv:hep-ph/0405172]; G. L. Fogli, E. Lisi, A. Marrone and A. Palazzo, Prog. Part. Nucl. Phys. **57** (2006) 742 [arXiv:hep-ph/0506083].
- [19] C. E. Yaguna, Int. J. Mod. Phys. A **21** (2006) 1283 [arXiv:hep-ph/0502014].
- [20] W. J. Marciano and A. I. Sanda, Phys. Rev. Lett. **38** (1977) 1512; G. Altarelli, L. Baulieu, N. Cabibbo, L. Maiani and R. Petronzio, Nucl. Phys. B **125** (1977) 285 [Erratum-ibid. B **130** (1977) 516]; M. Raidal and A. Santamaria, Phys. Lett. B **421** (1998) 250 [arXiv:hep-ph/9710389].
- [21] Z. Maki, M. Nakagawa and S. Sakata, Prog. Theor. Phys. **28** (1962) 870.

- [22] B. Pontecorvo, Sov. Phys. JETP **6** (1957) 429 [Zh. Eksp. Teor. Fiz. **33** (1957) 549]; Sov. Phys. JETP **7** (1958) 172 [Zh. Eksp. Teor. Fiz. **34** (1957) 247].
- [23] J. A. Casas and A. Ibarra, Nucl. Phys. B **618** (2001) 171 [arXiv:hep-ph/0103065].
- [24] J. D. Vergados, Phys. Rept. **133** (1986) 1; J. Bernabeu, E. Nardi and D. Tommasini, Nucl. Phys. B **409** (1993) 69 [arXiv:hep-ph/9306251]; A. Faessler, T. S. Kosmas, S. Kovalenko and J. D. Vergados, arXiv:hep-ph/9904335.
- [25] T. S. Kosmas, S. Kovalenko and I. Schmidt, Phys. Lett. B **511** (2001) 203 [arXiv:hep-ph/0102101].
- [26] H. C. Chiang, E. Oset, T. S. Kosmas, A. Faessler and J. D. Vergados, Nucl. Phys. A **559** (1993) 526.
- [27] E. Arganda, A. M. Curiel, M. J. Herrero and D. Temes, Phys. Rev. D **71** (2005) 035011 [arXiv:hep-ph/0407302].
- [28] A. Brignole and A. Rossi, Phys. Lett. B **566** (2003) 217 [arXiv:hep-ph/0304081]; Nucl. Phys. B **701** (2004) 3 [arXiv:hep-ph/0404211].
- [29] P. Paradisi, JHEP **0602** (2006) 050 [arXiv:hep-ph/0508054].
- [30] K. S. Babu and C. Kolda, Phys. Rev. Lett. **89** (2002) 241802 [arXiv:hep-ph/0206310].
- [31] B. C. Allanach *et al.*, in *Proc. of the APS/DPF/DPB Summer Study on the Future of Particle Physics (Snowmass 2001)* ed. N. Graf, Eur. Phys. J. C **25** (2002) 113 [eConf **C010630** (2001) P125] [arXiv:hep-ph/0202233].
- [32] W. Porod, Comput. Phys. Commun. **153** (2003) 275 [arXiv:hep-ph/0301101].
- [33] E. Arganda and M. J. Herrero, Phys. Rev. D **73** (2006) 055003 [arXiv:hep-ph/0510405].
- [34] S. Antusch, E. Arganda, M. J. Herrero and A. M. Teixeira, JHEP **0611** (2006) 090 [arXiv:hep-ph/0607263].
- [35] R. Kitano, M. Koike and Y. Okada, Phys. Rev. D **66** (2002) 096002 [arXiv:hep-ph/0203110].
- [36] M. Passera, Nucl. Phys. Proc. Suppl. **169** (2007) 213 [arXiv:hep-ph/0702027].
- [37] L. Calibbi, A. Faccia, A. Masiero and S. K. Vempati, arXiv:hep-ph/0605139.

- [38] F. Deppisch, T. S. Kosmas and J. W. F. Valle, Nucl. Phys. B **752** (2006) 80 [arXiv:hep-ph/0512360].
- [39] M. Blanke, A. J. Buras, B. Duling, A. Poschenrieder and C. Tarantino, JHEP **0705** (2007) 013 [arXiv:hep-ph/0702136].
- [40] E. Ables et al. [MINOS Collaboration], Fermilab-proposal-0875; G. S. Tzanakos [MINOS Collaboration], AIP Conf. Proc. 721 (2004) 179; M. Komatsu, P. Migliozzi and F. Terranova, J. Phys. G **29** (2003) 443 [arXiv:hep-ph/0210043]; P. Migliozzi and F. Terranova, Phys. Lett. B **563** (2003) 73 [arXiv:hep-ph/0302274]; P. Huber, J. Kopp, M. Lindner, M. Rolinec and W. Winter, JHEP **0605** (2006) 072 [arXiv:hep-ph/0601266]; Y. Itow *et al.*, arXiv:hep-ex/0106019; A. Blondel, A. Cervera-Villanueva, A. Donini, P. Huber, M. Mezzetto and P. Strolin, arXiv:hep-ph/0606111. P. Huber, M. Lindner, M. Rolinec and W. Winter, arXiv:hep-ph/0606119; J. Burguet-Castell, D. Casper, E. Couce, J. J. Gomez-Cadenas and P. Hernandez, Nucl. Phys. B **725** (2005) 306 [arXiv:hep-ph/0503021]; J. E. Campagne, M. Maltoni, M. Mezzetto and T. Schwetz, [arXiv:hep-ph/0603172].
- [41] W. Hollik, in *Precision Tests of the Standard Electroweak Model*, edited by P. Langacker (World Scientific, Singapore, 1995), pp. 37–116;
- [42] H. E. Haber and G. L. Kane, Phys. Rept. **117** (1985) 75.
- [43] J. F. Gunion and H. E. Haber, Nucl. Phys. B **272** (1986) 1 [Erratum-ibid. B **402** (1993) 567].